

# Low-depth amplitude estimation via statistical eigengap estimation

Po-Wei Huang<sup>1,2,\*</sup> and Bálint Koczor<sup>1,2,†</sup>

<sup>1</sup>*Mathematical Institute, University of Oxford, Woodstock Road, Oxford OX2 6GG, United Kingdom*

<sup>2</sup>*Quantum Motion, 9 Sterling Way, London N7 9HJ, United Kingdom*

(Dated: March 6, 2026)

Amplitude estimation, in its original form, is formulated as phase estimation upon the Grover walk operator. Since its introduction, subsequent improvements to the algorithm have removed the use of phase estimation and introduced low-depth variants that trade speedup factors for lower circuit depth. We make the key observation that amplitude estimation is equivalent to estimating the energy gap of an effective Hamiltonian, whereby discrete time evolution is generated by amplitude amplification. This enables us to develop two amplitude estimation algorithms for both Heisenberg-limited and low-depth circuit regimes, inspired by statistical phase estimation techniques developed for seemingly unrelated early fault-tolerant ground-state energy estimation. Our approach has significant technical and practical benefits, and uses simplified classical post-processing compared to prior techniques—our theoretical and numerical results indicate that we achieve state-of-the-art performance. Furthermore, while our approach achieves Heisenberg-limited scaling, we also establish optimal query-depth tradeoffs up to polylogarithmic factors in the low-depth regime with provable theoretical guarantees. Due to its flexibility, generality, and robustness, we expect our approach to be a key enabler for a broad range of early fault-tolerant applications.

**Introduction.**—The original amplitude estimation of Brassard *et al.* [1] applies phase estimation [2] to the amplitude amplification operator [3], but requires many controlled walk operations, ancilla qubits, and a quantum Fourier transform (QFT) [4]. Literature has focused on simplifying amplitude estimation, e.g., removing the phase estimation subroutine [5–11] and developing “low-depth” algorithms that trade off speedup factors for a lower circuit depth [8, 12, 13]. Independently, literature concerned with ground state energy estimation in Hamiltonian simulation focused on vastly improving conventional phase estimation by developing “statistical” variants of phase estimation that only require one ancilla qubit via the Hadamard test [2, 14] as relevant in early fault-tolerant applications [15–18]. Among those techniques, sampling from Gaussian filter functions has been shown to be effective for producing low-depth phase estimation algorithms [19–21]. We refer the reader to Appendix A for a summary of related work.

A natural question we ask is whether the statistical methods for phase estimation can provide efficient algorithms for both Heisenberg-limited and low-depth amplitude estimation. We answer this question by formulating amplitude estimation as an eigengap estimation problem, and provide two algorithms inspired by Gaussian-filtering-based statistical phase estimation, as shown in Fig. 1. For the first algorithm, we combine the usage of both “standard” amplitude amplification circuits and Loschmidt echo-esque circuits [22] with Gaussian filtering to achieve Heisenberg-limited amplitude estimation, while being limited to circuits with  $\Omega(a^{-\frac{1}{2}})$  depth in the low-depth regime, where  $a$  is the target amplitude. Our second algorithm applies to a special but still relatively broad class where

a flag qubit is used to indicate the good and bad subspaces. By applying Pauli X and Z measurements on the flag qubit after amplitude amplification, the algorithm achieves a low circuit depth that can be set arbitrarily and independently of the true amplitude, as shown by our theoretical guarantees.

**Key observation.**—Early fault-tolerant statistical phase estimation uses controlled time evolution operators and the Hadamard test [2, 14] to perform measurement on an ancillary qubit. Our theoretical results explain why, in contrast, state-of-the-art amplitude estimation algorithms (which do not use phase estimation) require no extra ancillary qubits, nor controlled evolutions [5–10], even in short depth regimes [12]. Specifically, in the following, we show that Grover’s amplitude amplification operator can be viewed as a discrete-time evolution under an effective Hamiltonian, and prove that amplitude estimation can be effectively formulated as a Hamiltonian energy gap estimation algorithm (rather than phase estimation), whereby expected values of observables are measured instead of the Hadamard test circuit.

**Quantum phase and eigengap estimation.**—First, let us recollect basics of phase estimation whereby one assumes that an  $K$ -dimensional Hamiltonian  $H$  with eigenvectors  $\{|\psi_i\rangle\}_{i\in[K]}$ , and an initial state  $|\psi\rangle = \sum_{i=1}^K c_i |\psi_i\rangle$  are given. By controlling the time evolution operator  $U_t = e^{-iHt}$  on a single ancilla qubit, its expected value can be estimated as the time series

$$\langle\psi|U_t|\psi\rangle = \sum_{k\in[K]} p_k e^{-itE_k}, \quad (1)$$

where  $p_k = |c_k|^2$  and  $\sum_{k\in[K]} p_k = 1$ . Classical frequency analysis of  $S(t) = \langle\psi|U_t|\psi\rangle$  allows us to obtain eigenvalues  $E_k$  that correspond to the dominant eigenvectors in the initial state.

\* po-wei.huang@maths.ox.ac.uk

† balint.koczor@maths.ox.ac.uk

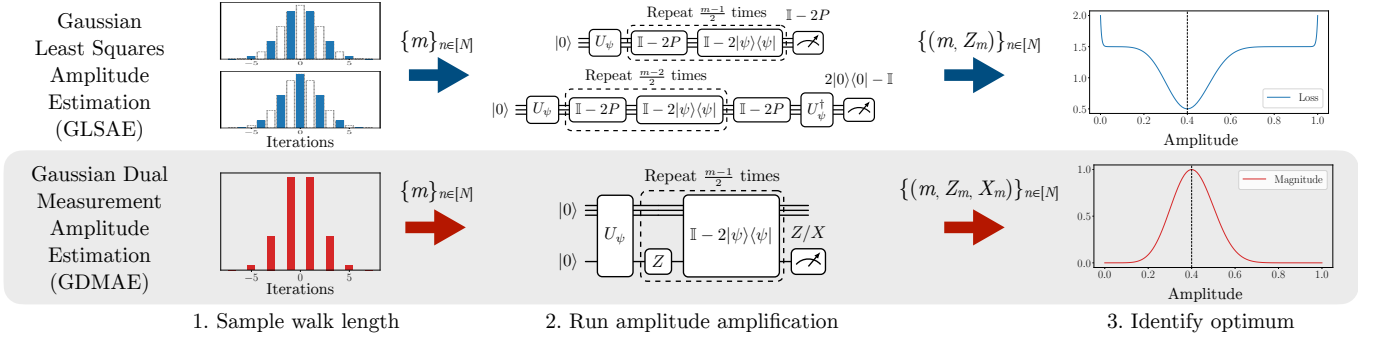


FIG. 1. *Overview.* We provide two algorithms for both Heisenberg-limited and low-depth amplitude estimation, utilizing techniques from early fault-tolerant statistical phase estimation algorithms. Both algorithms follow a simple three-step protocol. First, a series of  $\{m\}$  is sampled from a truncated discrete Gaussian. Second, we execute amplitude amplification circuits with  $m$  applications of  $U_\psi$ . Lastly, we construct a target function based on the measurement result for which the peak lies on an  $\epsilon$ -close estimate  $\tilde{a}$  of the target amplitude  $a = \|P|\psi\rangle\|^2$ .

In contrast, eigengap estimation is a resource-frugal alternative that requires no controlled time evolution or additional ancilla qubits, whereby time-evolved expected values of an observable  $O$  as

$$\langle \psi | U_t^\dagger O U_t | \psi \rangle = \sum_{j,k \in [K]} q_{j,k} e^{-it(E_k - E_j)}, \quad (2)$$

are estimated. Here  $q_{j,k} = c_j^* c_k \langle \psi_j | O | \psi_k \rangle$ . We select  $O$  suitably such that  $q_{j,k} = |q_{j,k}| e^{-i\theta_{j,k}}$  where  $\theta_{j,k}$  can be inferred and  $\sum_{j,k \in [K]} |q_{j,k}| = 1$ . The special case  $O = |\psi\rangle\langle\psi|$  yields the usual Loschmidt echo [22], which can be post-processed using statistical phase estimation techniques to obtain eigengaps, given  $\sum_{j,k \in [K]} q_{j,k} = 1$ .

Above, continuous time evolution  $U_t = e^{-itH}$  can be simulated with a range of techniques, including conventional [23–25] and randomized [26, 27] product formulas. However, for phase estimation, it may be more efficient to apply a discrete-time evolution  $U_t = e^{-itH}$  for  $t \in \mathbb{N}$  under an effective Hamiltonian—a prominent example is qubitization where  $U_t = e^{-itH_{\text{eff}}}$  with  $H_{\text{eff}} = \arccos(H/\Lambda)$  [28, 29], where  $\Lambda$  is a normalization factor. Phase estimation then reveals eigenvalues of the effective Hamiltonian  $H_{\text{eff}}$ , from which eigenvalues of the true Hamiltonian  $H$  follow via  $E_{\text{eff}} = \pm \arccos(E/\Lambda)$ . Qubitization enables state-of-the-art ground-state energy estimation [30, 31] and can, in principle, also be used to perform discrete-time evolution-based statistical phase estimation [21]. While our approach is similar in the sense that we apply a discrete-time evolution under an effective Hamiltonian, rather than extracting eigenvalues directly, our approach estimates eigengaps in the effective Hamiltonian through post-processing observable expected values.

**Amplitude amplification as discrete time evolution.**—Given a projector  $P$ , it decomposes the Hilbert space into a good subspace  $\mathcal{H}_G$  with  $P|\phi\rangle = |\phi\rangle$  and a bad subspace with  $P|\phi\rangle = \mathbf{0}$ . Given an arbitrary input state  $|\psi\rangle$ , the probability of measuring

it in the good subspace is  $a = \sin^2(\lambda) = \|P|\psi\rangle\|^2$  and we define the post-measurement states as  $|\psi_g\rangle = \frac{P|\psi\rangle}{\langle\psi|P|\psi\rangle}$  and  $|\psi_b\rangle = \frac{(\mathbb{I}-P)|\psi\rangle}{\langle\psi|\mathbb{I}-P|\psi\rangle}$ .

**Proposition 1** (Effective Hamiltonian of amplitude amplification). *We are given Grover’s walk operator  $Q = -(\mathbb{I}-2|\psi\rangle\langle\psi|)(\mathbb{I}-2P)$  for some arbitrary input state  $|\psi\rangle$  and a projector  $P$  such that  $a = \sin^2(\lambda) = \|P|\psi\rangle\|^2$ . Then  $Q$  is equivalent to a discrete-time evolution under an effective Hamiltonian  $H_{\text{eff}}$  where*

$$Q = e^{-iH_{\text{eff}}} \quad \text{with} \quad H_{\text{eff}} = -2\lambda Y_\psi + \pi(\mathbb{I}-P - |\psi_b\rangle\langle\psi_b|).$$

*In the 2-dimensional subspace  $\mathcal{H}_\psi = \text{span}\{|\psi_g\rangle, |\psi_b\rangle\}$ , the operator  $Y_\psi = i|\psi_b\rangle\langle\psi_g| - i|\psi_g\rangle\langle\psi_b|$  is an effective Pauli  $Y$  matrix, and therefore  $Q$  acts as a discrete Pauli  $Y$  rotation. In the subspace  $\mathcal{H}_\psi$ , the effective Hamiltonian has two eigenvalues which are related to the amplitude to be estimated as*

$$\pm E_{\text{eff}} = \pm 2\lambda = \pm 2 \arcsin(\sqrt{a}) = \pm \arccos(1 - 2a),$$

*where the last term uses the same convention as qubitization.*

We defer the proof to Appendix B1 and note the following points. First, conventional amplitude estimation proceeds by applying a discrete-time evolution under the effective Hamiltonian  $H_{\text{eff}}$  as part of phase estimation. Second, applying  $Q$  produces a nontrivial Pauli- $Y$  rotation  $e^{2\lambda Y_\psi}$  with eigenphases  $\pm \arccos(1 - 2a)$  in the subspace  $\mathcal{H}_\psi$ . Equivalently, projecting  $R = U^\dagger(\mathbb{I} - 2P)U$  onto the zero subspace gives  $\langle 0 | R | 0 \rangle = 1 - 2a$ . This provides the eigenvalues  $e^{\pm i \arccos(1 - 2a)}$  of  $U^\dagger(\mathbb{I} - 2P)U(2|0\rangle\langle 0| - \mathbb{I})$  per qubitization [32], which shares eigenvalues with  $Q$  by unitary invariance.

**Amplitude estimation as eigengap estimation.**—Rather than estimating the desired amplitude via phase estimation, one can instead apply more resource-efficient eigengap estimation to extract the energy gap in the effective Hamiltonian. The main difference to conventional

gap estimation is that we apply discrete time evolution  $U_t := Q^t$  where  $t \in \mathbb{N}$  and that we measure two Pauli-like observables  $O = \mathbb{I} - 2P$  and the observable corresponding to a shifted Loschmidt echo  $O' = 2|\psi\rangle\langle\psi| - \mathbb{I}$ .

**Proposition 2** (Effective Hamiltonian eigengap estimation). *Given the discrete time evolution operator  $U_t := Q^t$  under the effective Hamiltonian  $H_{\text{eff}}$  from Proposition 1, the expected value of the Pauli-like observable  $O = \mathbb{I} - 2P$  yields the time-dependent expected value in Eq. (2)*

$$\begin{aligned} \langle\psi|U_t^\dagger O U_t|\psi\rangle &= \sum_{E_j, E_k \in \{\pm E_{\text{eff}}\}} q_{j,k} e^{-it(E_j - E_k)} \\ &= \frac{e^{i2\lambda}}{2} e^{it\Delta_{\text{eff}}} + \frac{e^{-i2\lambda}}{2} e^{-it\Delta_{\text{eff}}} \end{aligned}$$

which depends on the effective Hamiltonian's energy gap  $\Delta_{\text{eff}} = 2E_{\text{eff}} = 4\lambda = 4 \arcsin(\sqrt{a})$ . Alternatively, using the observable  $O' = 2|\psi\rangle\langle\psi| - \mathbb{I}$ , we obtain the time series

$$\langle\psi|U_t^\dagger O' U_t|\psi\rangle = \frac{1}{2} e^{it\Delta_{\text{eff}}} + \frac{1}{2} e^{-it\Delta_{\text{eff}}}.$$

We defer the proof to Appendix B 2. The use of the shifted Loschmidt echo, in addition to the ‘‘standard’’ amplitude amplification circuit, is reminiscent of the use of even degree Chebyshev polynomials in amplitude estimation in the context of quantum signal processing [8]. Finally, we note that the last state reflection in  $Q^t$  may be omitted by replacing  $Q^t$  with  $(\mathbb{I} - 2P)Q^{t-1}$ , as the final measurement is performed on  $|\psi\rangle$  and the reflection by  $|\psi\rangle$  has no effect.

**Result 1: Gaussian-filtered ancilla-free amplitude estimation.**— The expected value of the time-evolved observable measurement in Proposition 2 is trivially related to the discrete-time signal  $S(m) = \cos(2\lambda m)$  for  $m \in \mathbb{Z}$ , i.e., averaging individual shots  $Z_m \in \{\pm 1\}$  of observable measurements yields the mean  $\mathbb{E}[Z_m|m] = \cos(2\lambda m)$ . Specifically, for odd  $m$ , we measure  $O = \mathbb{I} - 2P$  per Proposition 2 and set  $m = 2(t + \frac{1}{2})$ , while for even  $m$ , we measure  $O = 2|\psi\rangle\langle\psi| - \mathbb{I}$  and set  $m = 2t$ . The circuit depth is directly proportional to  $m$ , which we can limit by sampling the evolution times  $m \leq M = \mathcal{O}(T)$  from a truncated discrete Gaussian distribution  $\tilde{p}_T$  which has standard deviation  $T$ —for practical purposes,  $M = 4T$  is a reasonable approximation.

For the sampled evolution time  $m$ , we measure the corresponding amplitude amplification circuit of depth  $\mathcal{O}(m)$  and record the measurement outcome  $Z_m$ —the measured  $Z_m$ -s would then act as a sparse, noisy cosine signal that induces a form of sparse discrete-time cosine transform [33] over the discrete Gaussian. Inspired by statistical phase estimation techniques [17, 19, 20], we consider the loss function as the mean square error between the observed signal and the ideal cosine signal as

$$\tilde{\mathcal{L}}(\theta) = \frac{1}{N} \sum_{m \sim \tilde{p}_T} (Z_m - \cos(2\theta m))^2, \quad (3)$$

whose minimum recovers the amplitude as  $\lambda \approx \arg \min_{\theta \in [0, \pi/2]} \tilde{\mathcal{L}}(\theta)$ . We term this approach Gaussian Least Squares Amplitude Estimation (GLSAE), which yields Heisenberg-limited scaling of total quantum resources (space-time volume).

By tuning the discrete Gaussian’s standard deviation  $T$  and truncation threshold  $M \in \mathcal{O}(T)$  (equivalently, the maximum circuit depth), we obtain a trade-off between circuit depth and the number of samples  $N$ —this enables low-depth amplitude estimation at an extreme end. However, the approach is ill conditioned when circuits are not sufficiently deep to resolve an  $a$  that is either approximately 0 or 1: As the cosine signal in Proposition 2 has two frequency peaks corresponding to minima of  $\tilde{\mathcal{L}}$  at  $\theta = \pm\lambda$ , a low standard deviation  $T$  of our Gaussian may cause a significant broadening of these two peaks. When the broadening is comparable to the distance between the two peaks, the minimum of  $\tilde{\mathcal{L}}$  is difficult to discern in the presence of sampling noise due to finite repetition. Consequently, as formalized below, the estimable range of  $a$  is constrained by  $T$  (equivalently  $M$ ) via the tuning  $\beta$  and range  $\zeta$  parameters.

**Theorem 3** (GLSAE). *Fix a tuning parameter  $\beta \in [0, 1]$ , a target precision  $\epsilon > 0$  and set the range parameter  $\zeta \in \tilde{\mathcal{O}}(\epsilon^{2-2\beta})$ . Then, with high probability, there exists a quantum algorithm GLSAE that outputs an estimate  $\tilde{a}$  of  $a = \|P|\psi\rangle\|^2$ , for any  $a \in [\zeta, 1 - \zeta]$ , such that  $|\tilde{a} - a| \leq \epsilon$ . Moreover, GLSAE requires a maximum circuit depth  $M \in \tilde{\mathcal{O}}(\epsilon^{-1+\beta})$  and  $N \in \tilde{\mathcal{O}}(\epsilon^{-2\beta})$  parallel circuit samples.*

The proof for this theorem, detailed in Appendix D, utilizes strong convexity and smoothness properties of the periodic Gaussian produced from the discrete-time cosine transform—which we derive in Appendix C—to provide quadratic upper and lower bounds. These properties, when coupled with Hoeffding bounds on the number of samples, provide a quadratic inequality that, when solved, reproduces the Zalka–Burchard lower bound of  $M^2 N \in \mathcal{O}(\epsilon^{-2})$  [34, 35] up to polylogarithmic factors found for low-depth amplitude estimation protocols [12]. Remarkably, our proof for discrete-time effective Hamiltonian evolution presents a single inequality for all circuit depths—in contrast, even in the context of conventional Hamiltonian simulation, prior literature focused on specific regimes of circuit depths and spectral gap bounds [20, 21].

Theorem 3 depends on a tunable free parameter  $\beta$ , which affects the polynomial scaling of the runtime with respect to a target precision  $\epsilon$  such that the number of queries to the state preparation unitary can be interpolated between the Heisenberg and standard quantum limit, i.e., precision scaling between  $\tilde{\mathcal{O}}(\epsilon^{-1})$  and  $\tilde{\mathcal{O}}(\epsilon^{-2})$ . In contrast, the following corollary focuses on the special case when our approach applies to all  $a$  and achieves the Heisenberg limit of both  $\tilde{\mathcal{O}}(\epsilon^{-1})$  circuit depth and total  $\tilde{\mathcal{O}}(\epsilon^{-1})$  state preparation queries.

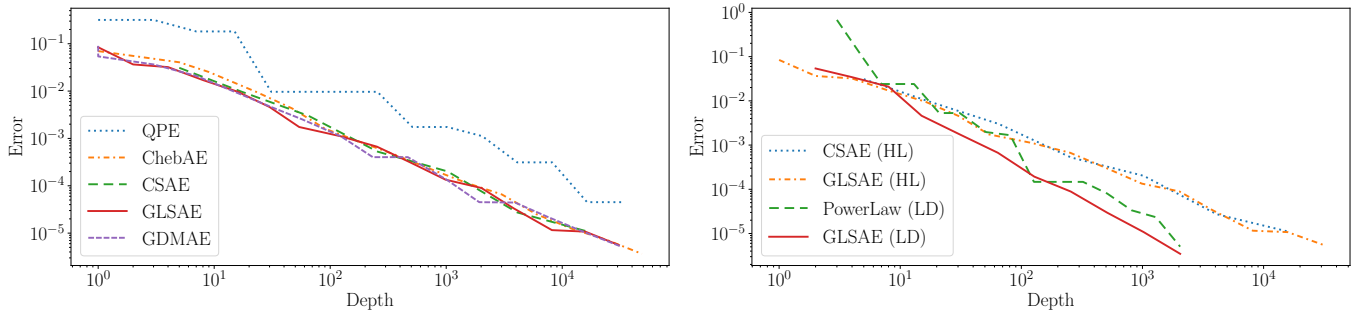


FIG. 2. Comparison of the circuit depth of near-Heisenberg-limited amplitude estimation algorithms (left) and low-depth amplitude estimation (right). GLSAE and GDMAE achieve state-of-the-art performance, comparable to ChebAE and CSAE. In the low-depth regime (right), we implement the case with circuit depth and sample complexity equivalent to uniform time sampling where  $M, N \in \tilde{\mathcal{O}}(\epsilon^{-2/3})$ . Our algorithm improves over prior art like Power law AE.

**Corollary 3.1.** Fixing  $\beta = 0$ , with high probability, GLSAE outputs an estimate  $\tilde{a}$  of  $a = \|P|\psi\rangle\|^2$ , for any  $a \in [0, 1]$ , such that  $|\tilde{a} - a| \leq \epsilon$ . GLSAE requires a maximum circuit depth  $M \in \tilde{\mathcal{O}}(\epsilon^{-1})$  and  $N \in \mathcal{O}(\log(\epsilon^{-1}))$  parallel circuit samples.

In the low-depth regime, while GLSAE can still be used to estimate up to  $\epsilon$  additive accuracy when  $a \in [\zeta, 1 - \zeta]$ , the range is much more limited. In other words, the lowest depth that we can achieve for true amplitude  $a$  is then  $\tilde{\mathcal{O}}(a^{-\frac{1}{2}})$ , providing a slight improvement over Rall and Fuller [8]. We resolve this limitation via the following strategy that exploits further structure.

**Result 2: Amplitude estimation using a flag qubit.**— In many practical scenarios, such as in quantum Monte Carlo [36, 37] and approximate counting [6] algorithms, as well as in quadratic speedups of Hadamard tests [14], we usually do not have a full description of the good  $|\psi_g\rangle$  and bad  $|\psi_b\rangle$  states. Still, a straightforward projector  $P$  for the good state is commonly achieved in such applications, whenever the state  $|\psi\rangle$  includes a flag qubit as

$$|\psi\rangle = \sin(\lambda)|\psi_g\rangle|1\rangle + \cos(\lambda)|\psi_b\rangle|0\rangle, \quad (4)$$

whose  $|0\rangle$  and  $|1\rangle$  states are coupled to the good and bad partitions. The projector is then simply  $P = \mathbb{I} \otimes |1\rangle\langle 1|$ , and we thus obtain the cosine signal  $S(m) = \cos(2\lambda m)$  via a single-qubit Pauli Z measurement on the flag qubit. This is, in fact, the setting for various amplitude estimation algorithms, even if the structural advantage provided by the flag qubit is not exploited [5–7, 10, 12].

As mentioned in the previous section, the range limit of GLSAE is formed by the broadening of twin Gaussian peaks as a result of only having access to cosine signals. To resolve this, we can make use of the flag qubit to obtain additional sine signals by replacing the Pauli Z measurement with Pauli X, such that

$$\langle\psi|Q^{-t}(\mathbb{I} \otimes X)Q^t|\psi\rangle = \sin((4t + 2)\lambda). \quad (5)$$

Cosine signals are symmetric, and their Fourier components at frequencies  $\theta = \pm\lambda$  are indistinguishable; however, including sine signals breaks this symmetry, and we

can thus uniquely identify a peak at  $\theta = \lambda$  even at low depths and under finite-repetition sampling noise.

As before, we sample evolution times, measure the Pauli Z and X operators, and record their outputs as  $Z_m$  and  $X_m$ . Maximizing the magnitude function

$$\tilde{\mathcal{M}}(\theta) = \frac{1}{N} \sum_{m \sim \tilde{q}_T} Z_m \cos(2\theta m) + X_m \sin(2\theta m), \quad (6)$$

under a truncated Gaussian  $\tilde{q}_T$  that provides samples for odd  $m = 2t + 1$ , we recover the desired amplitude  $\lambda \approx \arg \max_{\theta \in [0, \pi/2]} \tilde{\mathcal{M}}(\theta)$ . We term this method the Gaussian Dual Measurement Amplitude Estimation (GDMAE).  $\mathbb{E}[\tilde{\mathcal{M}}(\theta)]$  only has a single Gaussian peak at  $\theta = \lambda$  (up to periodicity  $\pi$ ); thus, the problem of overlapping peaks is resolved, and we obtain the following theorem.

**Theorem 4 (GDMAE).** Given a flag qubit as in Eq. (4), we can construct a quantum algorithm, GDMAE, that outputs  $\tilde{a}$  for all  $a \in [0, 1]$  such that  $|\tilde{a} - a| \leq \epsilon$  with the same asymptotic costs as Theorem 3 of a maximum circuit depth  $M \in \tilde{\mathcal{O}}(\epsilon^{-1+\beta})$  and  $N \in \tilde{\mathcal{O}}(\epsilon^{-2\beta})$  parallel circuit samples. Here, the parameter  $\beta \in [0, 1]$  can be chosen arbitrarily to interpolate between Heisenberg and standard shot-noise scalings.

We defer the proof of this theorem, which shares the same high-level idea as Theorem 3, to Appendix E. We remark that GDMAE measures two different Paulis on a flag qubit and may therefore look superficially similar to the Hadamard test. However, the Hadamard test estimates phase via controlled time evolution and an interferometric ancilla, while GDMAE targets the energy gap instead, requires no controlled evolution, and embeds the flag qubit in state preparation. The flag qubit approach is therefore not a variant of the Hadamard test, e.g., the distinction is even more apparent in quantum Monte Carlo mean estimation [36], where a binary random variable is amplitude-encoded onto the flag qubit via controlled rotations (see Appendix E).

**Numerics.**—We benchmark our algorithm against a broad range of prior amplitude estimation techniques, including “textbook” amplitude estimation that uses phase

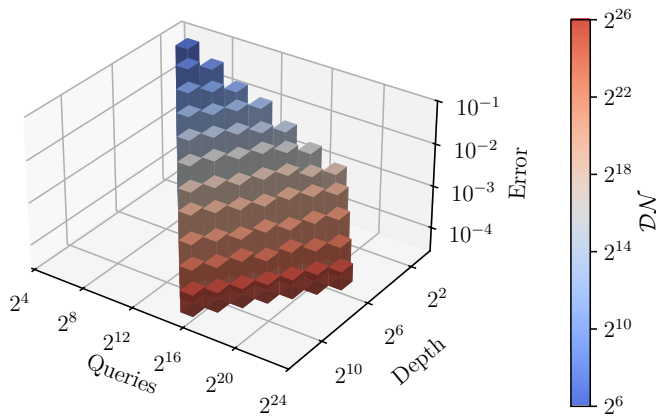


FIG. 3. *Depth–query invariance of low-depth amplitude estimation.* We show depth–query invariance of running GLSAE on low-depth amplitude amplification circuits. Varying the depth  $\mathcal{D}$  and query  $\mathcal{N}$  counts yields estimates of approximately identical precision as long as the product  $\mathcal{DN}$  is fixed.

estimation [1], ChebAE from quantum signal processing [8], and CSAE as a modified version of ESPRIT [10]. We additionally benchmark against adaptations of other ideas in signal processing and statistical phase estimation, which we detail in Appendix F.

While Fig. 2 (left) confirms that our approach achieves state-of-the-art performance in the Heisenberg limit, comparable to that of ChebAE and CSAE, we also have the following significant conceptual and technical advantages. First, we share the ability with CSAE for high parallelization over ChebAE due to being a non-iterative algorithm. Second, we have a substantially simplified construction relative to CSAE—the latter relies on costly classical post-processing to achieve Heisenberg-limited scaling, whereby a virtual uniform signal array is constructed via iterative outer products of the measured results sampled from a sequence that increments exponentially. Furthermore, Fig. 2 (right) confirms that in the low-depth regime, our approach improves over prior art such as Power law AE [12].

Finally, we demonstrate the depth–query tradeoff of GLSAE at fixed target precision in Fig. 3. We compare different  $(\mathcal{D}, \mathcal{N})$  pairs, where  $\mathcal{D}$  denotes the maximum depth and  $\mathcal{N}$  the total number of queries, rather than the parallel circuit count  $N$  and depth  $M$  used in the main proof, to account for practically relevant quantum resources and align with prior art. Indeed, as long as the product is fixed  $\mathcal{DN}$ , the estimation error is approximately constant (identical height bars in Fig. 3). While prior low-depth amplitude estimation algorithms required restrictive depth schedules [12], strong regularity assumptions [12], or restrictions on the biasedness of the quantum estimator [8, 13], our approach achieves the query–depth tradeoff  $\mathcal{DN} \in \tilde{\mathcal{O}}(\epsilon^{-2})$  with a simple and efficient single-variable post-processing optimization protocol.

**Discussion.**—In this work, we formulate amplitude estimation as eigengap estimation and develop two Gaussian-filtered algorithms achieving both Heisenberg-limited and low-depth resource scalings. While our approach has significant technical and practical advantages over prior amplitude estimation techniques, we numerically demonstrate in both circuit-depth regimes that we achieve state-of-the-art performance. Furthermore, our low-depth algorithm supports a query–depth tradeoff in terms of runtime speedups.

An open question concerns whether the minimum-depth limitation of GLSAE can be overcome without exploiting a flag qubit like GDMAE. Certain amplitude estimation tasks, such as observable estimation [38], lack this additional qubit and therefore cannot directly use GDMAE. A possible workaround is to introduce an ancillary qubit via the Hadamard test or, using only Loschmidt echo circuits, apply a multi-qubit Toffoli controlled on the main register, and perform Pauli measurements on the ancilla. Whether this ancilla qubit is required remains an open question. Although theoretical guarantees of GLSAE fail when the phase  $\lambda$  is near 0 or  $\frac{\pi}{2}$ , the sign of the sine function can, in principle, be inferred from the proximity and its magnitude recovered from the cosine (e.g.,  $\sqrt{1 - \cos^2 x}$  or a Hilbert transform). However, obtaining concentration bounds for the sine estimate via this inference method is nontrivial, and it remains uncertain whether such bounds would preserve the query–depth tradeoff invariance.

Due to the flexibility, generality, and robustness of our approach, we expect it will be a key enabler for a broad range of early fault-tolerant applications, such as expected value estimation, mean estimation, and beyond [6, 14, 36, 37].

**Code and Data Availability.**—The source code and data for numerics can be found at [https://github.com/georgepwhuang/qae\\_with\\_spe](https://github.com/georgepwhuang/qae_with_spe).

**Acknowledgements.**—The authors thank Hamza Jnane, Joshua Dai, Tom Bromley, and Simon Benjamin for discussions. PWH acknowledges support from the Engineering and Physical Sciences Research Council (EPSRC) Doctoral Training Partnership (EP/W524311/1) with a CASE Conversion Studentship in collaboration with Quantum Motion. PWH further acknowledges support from the Ministry of Education, Taiwan, for a Government Scholarship to Study Abroad (GSSA) and St. Catherine’s College, University of Oxford, for an Alan Tayer Scholarship. BK thanks UKRI for the Future Leaders Fellowship Theory to Enable Practical Quantum Advantage (MR/Y015843/1). BK also acknowledges funding from the EPSRC project Robust and Reliable Quantum Computing (RoaRQ, EP/W032635/1). For the purpose of Open Access, the author has applied a CC BY public copyright license to any Author Accepted Manuscript version arising from this submission.

- 
- [1] G. Brassard, P. Høyer, M. Mosca, and A. Tapp, Quantum amplitude amplification and estimation, in *Quantum computation and information*, Contemporary Mathematics, Vol. 305 (American Mathematical Society, Providence, RI, USA, 2002) pp. 53–74.
- [2] A. Y. Kitaev, Quantum measurements and the abelian stabilizer problem (1995), [arXiv:quant-ph/9511026](https://arxiv.org/abs/quant-ph/9511026) [quant-ph].
- [3] L. K. Grover, A fast quantum mechanical algorithm for database search, in *Proceedings of the Twenty-Eighth Annual ACM Symposium on Theory of Computing*, STOC '96 (Association for Computing Machinery, New York, NY, USA, 1996) p. 212–219.
- [4] D. Coppersmith, *An approximate Fourier transform useful in quantum factoring*, Tech. Rep. (IBM Research Division, 1994).
- [5] Y. Suzuki, S. Uno, R. Raymond, T. Tanaka, T. Onodera, and N. Yamamoto, Amplitude estimation without phase estimation, *Quantum Inf. Process.* **19** (2020).
- [6] S. Aaronson and P. Rall, Quantum approximate counting, simplified, in *Symposium on Simplicity in Algorithms* (Society for Industrial and Applied Mathematics, 2020) p. 24–32.
- [7] D. Grinko, J. Gacon, C. Zoufal, and S. Woerner, Iterative quantum amplitude estimation, *npj Quantum Inf.* **7** (2021).
- [8] P. Rall and B. Fuller, Amplitude estimation from quantum signal processing, *Quantum* **7**, 937 (2023).
- [9] R. Venkateswaran and R. O'Donnell, Quantum approximate counting with nonadaptive Grover iterations, in *38th International Symposium on Theoretical Aspects of Computer Science (STACS 2021)*, Leibniz International Proceedings in Informatics (LIPIcs), Vol. 187, edited by M. Bläser and B. Monmege (Schloss Dagstuhl – Leibniz-Zentrum für Informatik, Dagstuhl, Germany, 2021) pp. 59:1–59:12.
- [10] F. Labib, B. D. Clader, N. Stamatopoulos, and W. J. Zeng, Quantum amplitude estimation from classical signal processing (2024), [arXiv:2405.14697](https://arxiv.org/abs/2405.14697) [quant-ph].
- [11] Y. Yang and R. Yang, Classical postprocessing approach for quantum amplitude estimation, *Phys. Rev. A* **112**, 012625 (2025).
- [12] T. Giurgica-Tiron, I. Kerenidis, F. Labib, A. Prakash, and W. Zeng, Low depth algorithms for quantum amplitude estimation, *Quantum* **6**, 745 (2022).
- [13] D.-L. Vu, B. Cheng, and P. Rebentrost, Low-depth amplitude estimation without really trying, *ACM Trans. Quantum Comput.* **6** (2025).
- [14] R. Cleve, A. Ekert, C. Macchiavello, and M. Mosca, Quantum algorithms revisited, *Proc. R. Soc. Lond., A: Math. Phys. Eng. Sci.* **454**, 339 (1998).
- [15] L. Lin and Y. Tong, Heisenberg-limited ground-state energy estimation for early fault-tolerant quantum computers, *PRX Quantum* **3**, 010318 (2022).
- [16] K. Wan, M. Berta, and E. T. Campbell, Randomized quantum algorithm for statistical phase estimation, *Phys. Rev. Lett.* **129**, 030503 (2022).
- [17] Z. Ding and L. Lin, Even shorter quantum circuit for phase estimation on early fault-tolerant quantum computers with applications to ground-state energy estimation, *PRX Quantum* **4**, 020331 (2023).
- [18] H. Ni, H. Li, and L. Ying, On low-depth algorithms for quantum phase estimation, *Quantum* **7**, 1165 (2023).
- [19] G. Wang, D. S. França, R. Zhang, S. Zhu, and P. D. Johnson, Quantum algorithm for ground state energy estimation using circuit depth with exponentially improved dependence on precision, *Quantum* **7**, 1167 (2023).
- [20] Z. Ding and L. Lin, Simultaneous estimation of multiple eigenvalues with short-depth quantum circuit on early fault-tolerant quantum computers, *Quantum* **7**, 1136 (2023).
- [21] Z. Ding, H. Li, L. Lin, H. Ni, L. Ying, and R. Zhang, Quantum multiple eigenvalue Gaussian filtered search: an efficient and versatile quantum phase estimation method, *Quantum* **8**, 1487 (2024).
- [22] A. Goussev, R. A. Jalabert, H. M. Pastawski, and D. Wisniacki, Loschmidt echo, *Scholarpedia* **7**, 11687 (2012).
- [23] H. F. Trotter, On the product of semi-groups of operators, *Proc. Am. Math. Soc.* **10**, 545–551 (1959).
- [24] M. Suzuki, Generalized Trotter's formula and systematic approximants of exponential operators and inner derivations with applications to many-body problems, *Commun. Math. Phys.* **51**, 183–190 (1976).
- [25] M. Suzuki, General theory of fractal path integrals with applications to many-body theories and statistical physics, *J. Math. Phys.* **32**, 400–407 (1991).
- [26] E. Campbell, Random compiler for fast Hamiltonian simulation, *Phys. Rev. Lett.* **123**, 070503 (2019).
- [27] C. Kiumi and B. Koczor, TE-PAI: exact time evolution by sampling random circuits, *Quantum Sci. Technol.* **10**, 045071 (2025).
- [28] G. H. Low and I. L. Chuang, Hamiltonian simulation by qubitization, *Quantum* **3**, 163 (2019).
- [29] A. M. Childs, On the relationship between continuous- and discrete-time quantum walk, *Commun. Math. Phys.* **294**, 581–603 (2009).
- [30] D. W. Berry, C. Gidney, M. Motta, J. R. McClean, and R. Babbush, Qubitization of arbitrary basis quantum chemistry leveraging sparsity and low rank factorization, *Quantum* **3**, 208 (2019).
- [31] G. H. Low, R. King, D. W. Berry, Q. Han, A. E. DePrince, A. F. White, R. Babbush, R. D. Somma, and N. C. Rubin, Fast quantum simulation of electronic structure by spectral amplification, *Phys. Rev. X* **15**, 041016 (2025).
- [32] G. H. Low and I. L. Chuang, Optimal Hamiltonian simulation by quantum signal processing, *Phys. Rev. Lett.* **118**, 010501 (2017).
- [33] A. V. Oppenheim, R. W. Schaefer, M. A. Yoder, and W. T. Padgett, *Discrete-time signal processing*, 3rd ed. (Pearson, Upper Saddle River, NJ, 2009).
- [34] C. Zalka, Grover's quantum searching algorithm is optimal, *Phys. Rev. A* **60**, 2746 (1999).
- [35] P. Burchard, Lower bounds for parallel quantum counting (2019), [arXiv:1910.04555](https://arxiv.org/abs/1910.04555) [quant-ph].
- [36] A. Montanaro, Quantum speedup of Monte Carlo methods, *Proc. R. Soc. A: Math. Phys. Eng. Sci.* **471**, 20150301 (2015).
- [37] R. Kothari and R. O'Donnell, Mean estimation when you have the source code; or, quantum Monte Carlo methods, in *Proceedings of the 2023 Annual ACM-SIAM Symposium on Discrete Algorithms (SODA)* (Society for Industrial and Applied Mathematics, 2023) pp. 1186–1215.

- [38] E. Knill, G. Ortiz, and R. D. Somma, Optimal quantum measurements of expectation values of observables, *Phys. Rev. A* **75**, 012328 (2007).
- [39] P. Rebentrost, B. Gupt, and T. R. Bromley, Quantum computational finance: Monte Carlo pricing of financial derivatives, *Phys. Rev. A* **98**, 022321 (2018).
- [40] N. Stamatopoulos, D. J. Egger, Y. Sun, C. Zoufal, R. Iten, N. Shen, and S. Woerner, Option pricing using quantum computers, *Quantum* **4**, 291 (2020).
- [41] D. J. Egger, R. Garcia Gutierrez, J. C. Mestre, and S. Woerner, Credit risk analysis using quantum computers, *IEEE Trans. Comput.* **70**, 2136 (2021).
- [42] S. Woerner and D. J. Egger, Quantum risk analysis, *npj Quantum Inf.* **5** (2019).
- [43] S. Chakrabarti, R. Krishnakumar, G. Mazzola, N. Stamatopoulos, S. Woerner, and W. J. Zeng, A threshold for quantum advantage in derivative pricing, *Quantum* **5**, 463 (2021).
- [44] I. Kassal, S. P. Jordan, P. J. Love, M. Mohseni, and A. Aspuru-Guzik, Polynomial-time quantum algorithm for the simulation of chemical dynamics, *Proc. Natl. Acad. Sci. U.S.A.* **105**, 18681–18686 (2008).
- [45] T. E. O’Brien, M. Streif, N. C. Rubin, R. Santagati, Y. Su, W. J. Huggins, J. J. Goings, N. Moll, E. Kyoseva, M. Degroote, C. S. Tautermann, J. Lee, D. W. Berry, N. Wiebe, and R. Babbush, Efficient quantum computation of molecular forces and other energy gradients, *Phys. Rev. Res.* **4**, 043210 (2022).
- [46] P.-W. Huang, G. Boyd, G.-L. R. Anselmetti, M. Degroote, N. Moll, R. Santagati, M. Streif, B. Ries, D. Marti-Dafcik, H. Jnane, S. Simon, N. Wiebe, T. R. Bromley, and B. Koczor, Fullqubit alchemist: Quantum algorithm for alchemical free energy calculations (2025), [arXiv:2508.16719](https://arxiv.org/abs/2508.16719) [quant-ph].
- [47] J. van Apeldoorn and A. Gilyén, Quantum algorithms for zero-sum games (2019), [arXiv:1904.03180](https://arxiv.org/abs/1904.03180) [quant-ph].
- [48] P.-W. Huang and P. Rebentrost, Quantum algorithm for large-scale market equilibrium computation, in *Advances in Neural Information Processing Systems*, Vol. 37, edited by A. Globerson, L. Mackey, D. Belgrave, A. Fan, U. Paquet, J. Tomczak, and C. Zhang (Curran Associates, Inc., 2024) pp. 10878–10907.
- [49] N. Wiebe, A. Kapoor, and K. M. Svore, Quantum algorithms for nearest-neighbor methods for supervised and unsupervised learning, *Quantum Inf. Comput.* **15**, 316–356 (2015).
- [50] N. Wiebe, A. Kapoor, and K. M. Svore, Quantum deep learning, *Quantum Inf. Comput.* **16**, 541–587 (2016).
- [51] I. Kerenidis, J. Landman, A. Luongo, and A. Prakash, q-means: A quantum algorithm for unsupervised machine learning, in *Advances in Neural Information Processing Systems*, Vol. 32, edited by H. Wallach, H. Larochelle, A. Beygelzimer, F. d’Alché-Buc, E. Fox, and R. Garnett (Curran Associates, Inc., 2019).
- [52] I. Kerenidis, J. Landman, and A. Prakash, Quantum algorithms for deep convolutional neural networks, in *International Conference on Learning Representations* (2020).
- [53] I. Kerenidis and A. Prakash, Quantum gradient descent for linear systems and least squares, *Phys. Rev. A* **101**, 022316 (2020).
- [54] I. Kerenidis and A. Prakash, A quantum interior point method for LPs and SDPs, *ACM Trans. Quantum Comput.* **1** (2020).
- [55] J. van Apeldoorn, A. Gilyén, S. Gribling, and R. de Wolf, Quantum SDP-solvers: Better upper and lower bounds, *Quantum* **4**, 230 (2020).
- [56] A. Sidford and C. Zhang, Quantum speedups for stochastic optimization, in *Advances in Neural Information Processing Systems*, Vol. 36, edited by A. Oh, T. Naumann, A. Globerson, K. Saenko, M. Hardt, and S. Levine (Curran Associates, Inc., 2023) pp. 35300–35330.
- [57] S. Pillai, Y. Bar-Ness, and F. Haber, A new approach to array geometry for improved spatial spectrum estimation, *Proc. IEEE* **73**, 1522 (1985).
- [58] R. Roy and T. Kailath, ESPRIT-estimation of signal parameters via rotational invariance techniques, *IEEE Trans. Acoust. Speech Signal Process.* **37**, 984 (1989).
- [59] C.-L. Liu and P. P. Vaidyanathan, Remarks on the spatial smoothing step in coarray MUSIC, *IEEE Signal Process. Lett.* **22**, 1438 (2015).
- [60] E. T. Campbell, Early fault-tolerant simulations of the Hubbard model, *Quantum Sci. Technol.* **7**, 015007 (2021).
- [61] A. Katabarwa, K. Gratsea, A. Caesura, and P. D. Johnson, Early fault-tolerant quantum computing, *PRX Quantum* **5**, 020101 (2024).
- [62] T. Giurgica-Tiron, S. Johri, I. Kerenidis, J. Nguyen, N. Pienti, A. Prakash, K. Sosnova, K. Wright, and W. Zeng, Low-depth amplitude estimation on a trapped-ion quantum computer, *Phys. Rev. Res.* **4**, 033034 (2022).
- [63] J. van Apeldoorn, A. Cornelissen, A. Gilyén, and G. Nannicini, Quantum tomography using state-preparation unitaries, in *Proceedings of the 2023 Annual ACM-SIAM Symposium on Discrete Algorithms (SODA)* (Society for Industrial and Applied Mathematics, 2023) pp. 1265–1318.
- [64] A. Cornelissen and Y. Hamoudi, A sublinear-time quantum algorithm for approximating partition functions, in *Proceedings of the 2023 Annual ACM-SIAM Symposium on Discrete Algorithms (SODA)* (Society for Industrial and Applied Mathematics, 2023) pp. 1245–1264.
- [65] K. Oshio, K. Wada, and N. Yamamoto, Near-Heisenberg-limited parallel amplitude estimation with logarithmic depth circuit (2025), [arXiv:2508.06121](https://arxiv.org/abs/2508.06121) [quant-ph].
- [66] J. M. Martyn, Z. M. Rossi, K. Z. Cheng, Y. Liu, and I. L. Chuang, Parallel quantum signal processing via polynomial factorization, *Quantum* **9**, 1834 (2025).
- [67] J. S. Nelson and A. D. Baczewski, Assessment of quantum phase estimation protocols for early fault-tolerant quantum computers, *Phys. Rev. A* **110**, 042420 (2024).
- [68] O. Kiss, U. Azad, B. Requena, A. Roggero, D. Wakeham, and J. M. Arrazola, Early fault-tolerant quantum algorithms in practice: Application to ground-state energy estimation, *Quantum* **9**, 1682 (2025).
- [69] B. L. Higgins, D. W. Berry, S. D. Bartlett, M. W. Mitchell, H. M. Wiseman, and G. J. Pryde, Demonstrating Heisenberg-limited unambiguous phase estimation without adaptive measurements, *New J. Phys.* **11**, 073023 (2009).
- [70] S. Kimmel, G. H. Low, and T. J. Yoder, Robust calibration of a universal single-qubit gate set via robust phase estimation, *Phys. Rev. A* **92**, 062315 (2015).
- [71] F. Belliard and V. Giovannetti, Achieving Heisenberg scaling with maximally entangled states: An analytic upper bound for the attainable root-mean-square error, *Phys. Rev. A* **102**, 042613 (2020).
- [72] A. E. Russo, K. M. Rudinger, B. C. A. Morrison, and A. D. Baczewski, Evaluating energy differences on a quantum

- computer with robust phase estimation, *Phys. Rev. Lett.* **126**, 210501 (2021).
- [73] Y. Dong, L. Lin, and Y. Tong, Ground-state preparation and energy estimation on early fault-tolerant quantum computers via quantum eigenvalue transformation of unitary matrices, *PRX Quantum* **3**, 040305 (2022).
- [74] G. Wang, D. S. França, G. Rendon, and P. D. Johnson, Efficient ground-state-energy estimation and certification on early fault-tolerant quantum computers, *Phys. Rev. A* **111**, 012426 (2025).
- [75] R. D. Somma, Quantum eigenvalue estimation via time series analysis, *New J. Phys.* **21**, 123025 (2019).
- [76] A. Dutkiewicz, B. M. Terhal, and T. E. O'Brien, Heisenberg-limited quantum phase estimation of multiple eigenvalues with few control qubits, *Quantum* **6**, 830 (2022).
- [77] Y. Hua and T. Sarkar, Matrix pencil method for estimating parameters of exponentially damped/undamped sinusoids in noise, *IEEE Trans. Acoust. Speech Signal Process.* **38**, 814 (1990).
- [78] T. Sarkar and O. Pereira, Using the matrix pencil method to estimate the parameters of a sum of complex exponentials, *IEEE Antennas Propag. Mag.* **37**, 48 (1995).
- [79] M. E. Stroeks, J. Helsen, and B. M. Terhal, Spectral estimation for Hamiltonians: a comparison between classical imaginary-time evolution and quantum real-time evolution, *New J. Phys.* **24**, 103024 (2022).
- [80] H. Li, H. Ni, and L. Ying, Adaptive low-depth quantum algorithms for robust multiple-phase estimation, *Phys. Rev. A* **108**, 062408 (2023).
- [81] Z. Ding, E. N. Epperly, L. Lin, and R. Zhang, The ESPRIT algorithm under high noise: Optimal error scaling and noisy super-resolution, in *2024 IEEE 65th Annual Symposium on Foundations of Computer Science (FOCS)* (2024) pp. 2344–2366.
- [82] C. Yi, C. Zhou, and J. Takahashi, Quantum phase estimation by compressed sensing, *Quantum* **8**, 1579 (2024).
- [83] D. Castaldo and S. Corni, Heisenberg limited multiple eigenvalue estimation via off-the-grid compressed sensing (2025), [arXiv:2507.12438](https://arxiv.org/abs/2507.12438) [quant-ph].
- [84] E. J. Candes and T. Tao, Near-optimal signal recovery from random projections: Universal encoding strategies?, *IEEE Trans. Inf. Theory* **52**, 5406 (2006).
- [85] E. J. Candes, J. Romberg, and T. Tao, Robust uncertainty principles: exact signal reconstruction from highly incomplete frequency information, *IEEE Trans. Inf. Theory* **52**, 489 (2006).
- [86] Y. Pati, R. Rezaifar, and P. Krishnaprasad, Orthogonal matching pursuit: recursive function approximation with applications to wavelet decomposition, in *Proceedings of 27th Asilomar Conference on Signals, Systems and Computers* (1993) pp. 40–44 vol.1.
- [87] I. Zintchenko and N. Wiebe, Randomized gap and amplitude estimation, *Phys. Rev. A* **93**, 062306 (2016).
- [88] Y. Yang, A. Christianen, M. C. Bañuls, D. S. Wild, and J. I. Cirac, Phase-sensitive quantum measurement without controlled operations, *Phys. Rev. Lett.* **132**, 220601 (2024).
- [89] H. H. S. Chan, R. Meister, M. L. Goh, and B. Koczor, Algorithmic shadow spectroscopy, *PRX Quantum* **6**, 010352 (2025).
- [90] Y. Yang, Y. Li, X. Xu, and X. Yuan, Resource-efficient quantum-classical hybrid algorithm for energy gap evaluation, *Phys. Rev. A* **109**, 052416 (2024).
- [91] L. Clinton, T. S. Cubitt, R. Garcia-Patron, A. Montanaro, S. Stanisic, and M. Stroeks, Quantum phase estimation without controlled unitaries, *PRX Quantum* (2026).
- [92] Y. Nesterov, *Introductory Lectures on Convex Optimization: A Basic Course*, Applied Optimization (Springer New York, NY, 2004).
- [93] V. Giovannetti, S. Lloyd, and L. Maccone, Quantum metrology, *Phys. Rev. Lett.* **96**, 010401 (2006).
- [94] D. Wang, O. Higgott, and S. Brierley, Accelerated variational quantum eigensolver, *Phys. Rev. Lett.* **122**, 140504 (2019).
- [95] Y. Tong, A tight query complexity lower bound for phase estimation under circuit depth constraint (2021).
- [96] Z. Ding, Y. Dong, Y. Tong, and L. Lin, Robust ground-state energy estimation under depolarizing noise (2024), [arXiv:2307.11257](https://arxiv.org/abs/2307.11257) [quant-ph].
- [97] R. Tibshirani, Regression shrinkage and selection via the Lasso, *J. R. Stat. Soc.: B (Methodol.)* **58**, 267–288 (1996).
- [98] N. Derevianko, G. Plonka, and R. Razavi, ESPRIT versus ESPIRA for reconstruction of short cosine sums and its application, *Numer. Algorithms* **92**, 437–470 (2022).

# Appendices for “Low-depth amplitude estimation via statistical eigengap estimation”

## CONTENTS

|  |    |
|--|----|
| A. Related work  | 9  |
| 1. Amplitude estimation  | 9  |
| 2. Phase estimation  | 10 |
| B. An eigengap-based formulation of amplitude estimation                 | 10 |
| 1. Proof for amplitude amplification as discrete-time evolution          | 11 |
| 2. Proof for amplitude estimation as eigengap estimation                 | 11 |
| C. Analytical properties of the periodic Gaussian                        | 12 |
| 1. Local convexity of the periodic Gaussian                              | 13 |
| 2. Smoothness of the periodic Gaussian                                   | 13 |
| 3. Strongly concave areas of the periodic Gaussian                       | 15 |
| D. Further details on GLSAE  | 16 |
| 1. Algorithm and discussions for GLSAE                                   | 16 |
| 2. Proofs for GLSAE  | 18 |
| a. Truncation and sampling errors of the loss function                   | 19 |
| b. Main proof  | 21 |
| E. Further details on GDMAE  | 22 |
| 1. Algorithm and discussions for GDMAE                                   | 22 |
| 2. Proofs for GDMAE  | 24 |
| a. Construction and properties of the alternating-sign periodic Gaussian | 24 |
| b. Truncation and sampling errors of the magnitude function              | 25 |
| c. Main proof  | 26 |
| F. Implementation details for numerics                                   | 27 |
| 1. Heisenberg-limited amplitude estimation                               | 27 |
| 2. Low-depth amplitude estimation  | 29 |

### Appendix A: Related work

We now provide a summary of advancements in amplitude estimation and phase estimation in recent years.

#### 1. Amplitude estimation

Amplitude estimation [1] is a staple in designing quantum algorithms with Grover-type speedups [3], due to its formulation as a quadratic speedup over classical Monte Carlo algorithms [36]. Since its introduction, amplitude estimation has been used to provide quantum algorithms for various applications such as finance [39–43], quantum chemistry [38, 44–46], game theory [47, 48], machine learning [49–52], and optimization [53–56].

Following the original formulation, recent work has demonstrated that quantum amplitude estimation can achieve Heisenberg-limited performance without relying on quantum phase estimation. Suzuki *et al.* [5] first showed this by combining amplitude amplification with

maximum likelihood estimation, removing the need for both controlled walk operators and ancilla qubits. This work has been followed by multiple others that discard the use of phase estimation, including adaptive approaches [6] and iterative approaches [7, 8], as well as parallelizable approaches that apply classical post-processing [9–11].

Current state-of-the-art among these methods include ChebAE from quantum signal processing [8] and CSAE from a modified version of the classical signal processing algorithm ESPRIT (Estimation of Signal Parameters via Rotational Invariance Techniques) [10], which we include in the numerical comparisons to our algorithm. Chebyshev amplitude estimation, or ChebAE, modifies the Iterative Quantum Amplitude Estimation (IQAE) [7] such that the algorithm iteratively finds the higher Chebyshev polynomial of  $a$  implementable by Grover iterates or quantum signal processing (QSP) circuits [32] for measurement to shrink the confidence interval of the amplitude estimate  $\tilde{a}$ . Amplitude estimation from classical signal processing, or CSAE, on the other hand, opts for an approach where measurements on an exponentially incremental sequence

are used to interpolate and generate virtual signals that form a uniform signal grid via iterative outer products of the measurement and virtual signals from the previous iteration [57]. After generating the uniform linear array of signals, a modified version of the classical signal processing algorithm ESPRIT for direction of arrival problems [58, 59] is applied to recover the associated phase  $\lambda$  from the input signals.

Other efforts have been made in what is known as “low-depth” amplitude estimation algorithms. Giurgica-Tiron *et al.* [12] provided two such algorithms that showed that it is possible to trade off some of the quadratic speedup obtained by amplitude estimation for a lower circuit depth, paving the way for implementation in the early fault-tolerant regime [60–62]. Their first algorithm, Power law AE, uses power law schedules combined with Suzuki *et al.* [5]’s maximum likelihood estimation amplitude estimation to obtain low-depth circuits, providing an algorithm with practical functionality, but have theoretical guarantees are conditioned on strong regularity conditions that may not necessarily be present. The second algorithm, QoPrime amplitude estimation pieces estimates from several low-depth circuits together with the Chinese Remainder Theorem to obtain the value of  $a$ , but is restricted to discrete circuit depths of fractional powers of the inverse error. Though the QoPrime AE algorithm provides concrete theoretical guarantees, its performance have been shown to be inferior to Power law AE [12, 62]. Further, neither algorithm can be extended to work for the Heisenberg-limited regime.

Rall and Fuller [8] later proposed a low-depth algorithm that iteratively constructs (low-depth) semi-Pellian polynomial transformations of the encoded amplitude  $a$  by QSP and, from the measurement results, iteratively shrinks the confidence interval of the amplitude estimate  $\tilde{a}$ . Their algorithm has the caveat where it only operates when the circuit depth is of  $\Omega(a^{-1})$  where  $a$  is the true amplitude. Vu *et al.* [13] applied Monte Carlo estimation on top of separate individual runs of amplitude estimation with low circuit depth to aggregate the estimates, but requires the individual amplitude estimation algorithms to be unbiased [8, 63, 64]. Lastly, Oshio *et al.* [65] showed that it is possible to retain near Heisenberg-limited performance at low depths by preparing global GHZ states and parallelizing QSP circuits [66], but at a cost of high simultaneous qubit consumption and high initial all-to-all entanglement.

## 2. Phase estimation

While efforts have been made in amplitude estimation to remove phase estimation as a subroutine, phase estimation itself has been vastly simplified to versions that only require one ancilla qubit. These versions utilize the Hadamard test [2, 14] instead of the full circuit including QFT as an early fault-tolerant alternative [67, 68]. While Kitaev [2]’s original algorithm also featured a single an-

cilla qubit, the algorithm required exact eigenstates as input and lacks the robustness feature in more recent phase estimation algorithms. Lin and Tong [15] proposed a phase estimation algorithm that achieved the Heisenberg limit by constructing the cumulative distribution function of the spectral measure, and identifies “jumps” in the continuity as eigenvalues of the evolved Hamiltonian. Further work has been extended on what is now known as “statistical phase estimation” by introducing an improved Fourier series approximation and randomized Hamiltonian simulation [16]. By introducing Gaussian filter functions to sample evolution times, Wang *et al.* [19] were able to achieve low-depth circuits for phase estimation that traded the speedup of phase estimation with circuit depth. Alternative approaches [17, 18] inspired by robust phase estimation [69–72] that applied multi-level search for eigenvalues were able to produce similar low-depth results. Further development included algorithms that achieved further speedups on the dependency of overlap of the initial state [73], as well as its low-depth counterpart [74].

Similar approaches have also been applied to a generalized version of the phase estimation that involved extracting multiple eigenvalues from a single input state and Hamiltonian evolution operator. Somma [75] was the first to approach the task with the Hadamard test and treated the problem as a time-series analysis. Later works approached the generalized task by combining ideas from classical signal processing, including the matrix pencil method [76–78], ESPRIT [58, 79–81], and compressed sensing [82–85]. Building upon Gaussian filtering and combining with least squares minimization, Ding and Lin [20] were able to provide low-depth algorithms for the multiple eigenvalue estimation problem, which was later improved by Ding *et al.* [21] with a search method similar to orthogonal pursuit matching [86].

Lastly, eigengap estimation and ancilla-free phase estimation algorithms that discard the use of controlled unitaries and the ancilla qubit to have been explored by preparing equal superpositions as the initial state [72], injecting Haar random unitaries and obtaining the survival probability [87], combining real-time and imaginary-time evolution [88], utilizing classical shadows [89], introducing Gaussian filters [90], and adapting phase retrieval algorithms [91], with various caveats, limitations, and runtime sacrifices attached to each algorithm.

## Appendix B: An eigengap-based formulation of amplitude estimation

In this section, we expand on the details of the theoretical background of the main text and discuss relevant proofs.

### 1. Proof for amplitude amplification as discrete-time evolution

As mentioned in the main text, amplitude amplification can be written as a discrete-time evolution operator under some effective Hamiltonian  $H_{\text{eff}}$  such that for  $t \in \mathbb{N}$ ,

$$Q^t = \left( -(\mathbb{I} - 2|\psi\rangle\langle\psi|)(\mathbb{I} - 2P) \right)^t = e^{-itH_{\text{eff}}}. \quad (\text{B.1})$$

The following proposition from the main text and proof obtains  $H_{\text{eff}}$  and its eigenvalues.

**Proposition 1** (Effective Hamiltonian of amplitude amplification). *We are given Grover's walk operator  $Q = -(\mathbb{I} - 2|\psi\rangle\langle\psi|)(\mathbb{I} - 2P)$  for some arbitrary input state  $|\psi\rangle$  and a projector  $P$  such that  $a = \sin^2(\lambda) = \|P|\psi\rangle\|^2$ . Then  $Q$  is equivalent to a discrete-time evolution under an effective Hamiltonian  $H_{\text{eff}}$  where*

$$Q = e^{-iH_{\text{eff}}} \quad \text{with} \quad H_{\text{eff}} = -2\lambda Y_\psi + \pi(\mathbb{I} - P - |\psi_b\rangle\langle\psi_b|).$$

In the 2-dimensional subspace  $\mathcal{H}_\psi = \text{span}\{|\psi_g\rangle, |\psi_b\rangle\}$ , the operator  $Y_\psi = i|\psi_b\rangle\langle\psi_g| - i|\psi_g\rangle\langle\psi_b|$  is an effective Pauli  $Y$  matrix, and therefore  $Q$  acts as a discrete Pauli  $Y$  rotation. In the subspace  $\mathcal{H}_\psi$ , the effective Hamiltonian has two eigenvalues which are related to the amplitude to be estimated as

$$\pm E_{\text{eff}} = \pm 2\lambda = \pm 2 \arcsin(\sqrt{a}) = \pm \arccos(1 - 2a),$$

where the last term uses the same convention as qubitization.

*Proof.* The state  $|\psi\rangle$  can be decomposed into a good state and a bad state as follows:

$$|\psi\rangle = \sin(\lambda)|\psi_g\rangle + \cos(\lambda)|\psi_b\rangle, \quad (\text{B.2})$$

where

$$|\psi_g\rangle = \frac{P|\psi\rangle}{\sqrt{\langle\psi|P|\psi\rangle}}, \quad |\psi_b\rangle = \frac{(\mathbb{I} - P)|\psi\rangle}{\sqrt{\langle\psi|(\mathbb{I} - P)|\psi\rangle}}. \quad (\text{B.3})$$

Amplitude amplification is implemented by the walk operator (up to a global phase)

$$Q = -(\mathbb{I} - 2|\psi\rangle\langle\psi|)(\mathbb{I} - 2P), \quad (\text{B.4})$$

where repeated application induces a coherent rotation in the two-dimensional subspace  $\mathcal{H}_\psi = \text{span}\{|\psi_g\rangle, |\psi_b\rangle\}$  [1].

Restricting to  $\mathcal{H}_\psi$ , the operator  $Q$  acts as a real-valued rotation,

$$\begin{matrix} |\psi_g\rangle & & |\psi_b\rangle \\ |\psi_g\rangle & \begin{bmatrix} \cos(2\lambda) & \sin(2\lambda) \\ -\sin(2\lambda) & \cos(2\lambda) \end{bmatrix} & \\ |\psi_b\rangle & & \end{matrix} \quad (\text{B.5})$$

which may be identified as a Pauli- $Y$  rotation with angle  $-2\lambda$ . In the orthogonal complement space  $\mathcal{H}_\psi^\perp$ , we see that  $\mathbb{I} - 2|\psi\rangle\langle\psi|$  acts trivially, while  $-(\mathbb{I} - 2P)$  applies a phase  $-1$  to the bad subspace  $\mathcal{H}_B$ . With this, we have

constructed the spectrum for  $Q$  in both  $\mathcal{H}_\psi$  and  $\mathcal{H}_\psi^\perp$ . We can thus interpret  $Q$  as the discrete-time propagator generated by an effective Hamiltonian  $H_{\text{eff}}$ . Writing

$$Y_\psi = i|\psi_b\rangle\langle\psi_g| - i|\psi_g\rangle\langle\psi_b|, \quad (\text{B.6})$$

we may express  $Q = e^{-iH_{\text{eff}}}$  with

$$H_{\text{eff}} = -2\lambda Y_\psi + \pi(\mathbb{I} - P - |\psi_b\rangle\langle\psi_b|). \quad (\text{B.7})$$

The spectrum of  $H_{\text{eff}}$  consists of eigenvalues  $\{\pm 2\lambda, \pi, 0\}$ , with the nontrivial dynamics confined to  $\mathcal{H}_\psi$ . Under this construction, we see that amplitude amplification corresponds to discrete-time evolution under the effective Hamiltonian  $H_{\text{eff}}$ , and that  $Q$  has eigenvalues  $e^{\pm 2i\lambda}$  in subspace  $\mathcal{H}_\psi$ . Substituting  $a = \sin^2(\lambda)$ , we see that the eigenvalues are  $e^{\pm 2i \arcsin \sqrt{a}}$ .

To obtain the eigenvalue in the form of imaginary exponents of arccosines, we apply  $Q$  to the  $|\psi\rangle$  such that

$$\begin{aligned} Q|\psi\rangle &= -(\mathbb{I} - 2|\psi\rangle\langle\psi|)(\mathbb{I} - 2P)|\psi\rangle \\ &= -|\psi\rangle + 2|\psi\rangle + 2P|\psi\rangle - 4\langle\psi|P|\psi\rangle|\psi\rangle \\ &= (1 - 2a)|\psi\rangle + 2(P|\psi\rangle - \langle\psi|P|\psi\rangle|\psi\rangle) \end{aligned} \quad (\text{B.8})$$

where the latter term is orthogonal to  $|\psi\rangle$ . We then see that the eigenvalues of  $Q$  are  $e^{\pm i \arccos(1 - 2a)}$ , corresponding to conventions in literature on qubitization.

To provide these results in the qubitization picture [28], we can construct the reflection operator  $R = U^\dagger(\mathbb{I} - 2P)U$ . By applying qubitization over all qubits such that the entire Hilbert space is reduced to an effective 2-level system, we obtain the qubitized operator  $S$  such that

$$S = R(2|0\rangle\langle 0| - \mathbb{I}) = U^\dagger(\mathbb{I} - 2P)U(2|0\rangle\langle 0| - \mathbb{I}). \quad (\text{B.9})$$

To obtain the eigenvalues of the qubitized values, we first note that

$$\langle 0|U^\dagger(\mathbb{I} - 2P)U|0\rangle = 1 - 2\langle 0|U^\dagger P U|0\rangle = 1 - 2a. \quad (\text{B.10})$$

Thus, the eigenvalues of qubitized operator  $S$  is then  $e^{\pm i \arccos(1 - 2a)}$ . Noting that  $S = U^\dagger Q U$ , we see that by unitary invariance of eigenvalues, the eigenvalues of  $Q$  are also  $e^{\pm i \arccos(1 - 2a)}$ .  $\square$

### 2. Proof for amplitude estimation as eigengap estimation

Given the construction of amplitude amplification as a discrete-time evolution operator, where the eigenvalues of the effective Hamiltonian in the nontrivial subspace  $\mathcal{H}_\psi$  being  $\pm E_{\text{eff}} = \pm 2\lambda$ , the eigengap in this subspace is thus  $\Delta_{\text{eff}} = E_{\text{eff}} - (-E_{\text{eff}}) = 4\lambda$ . This can be extracted by eigengap estimation techniques, which forego the use of phase estimation, which requires at least an additional ancilla qubit and controlled time evolutions, aligning with amplitude estimation protocols without phase estimation [5–7, 9, 10].

**Proposition 2** (Effective Hamiltonian eigengap estimation). *Given the discrete time evolution operator  $U_t := Q^t$  under the effective Hamiltonian  $H_{\text{eff}}$  from [Proposition 1](#), the expected value of the Pauli-like observable  $O = \mathbb{I} - 2P$  yields the time-dependent expected value in [Eq. \(2\)](#)*

$$\begin{aligned} \langle \psi | U_t^\dagger O U_t | \psi \rangle &= \sum_{E_j, E_k \in \{\pm E_{\text{eff}}\}} q_{j,k} e^{-it(E_j - E_k)} \\ &= \frac{e^{i2\lambda}}{2} e^{it\Delta_{\text{eff}}} + \frac{e^{-i2\lambda}}{2} e^{-it\Delta_{\text{eff}}} \end{aligned}$$

which depends on the effective Hamiltonian's energy gap  $\Delta_{\text{eff}} = 2E_{\text{eff}} = 4\lambda = 4 \arcsin(\sqrt{a})$ . Alternatively, using the observable  $O' = 2|\psi\rangle\langle\psi| - \mathbb{I}$ , we obtain the time series

$$\langle \psi | U_t^\dagger O' U_t | \psi \rangle = \frac{1}{2} e^{it\Delta_{\text{eff}}} + \frac{1}{2} e^{-it\Delta_{\text{eff}}}.$$

*Proof.* From the fact that  $Q$  is a Pauli Y rotation in the subspace  $\mathcal{H}_\psi$ , we can see that  $Q$  has two eigenvectors in the subspace  $\mathcal{H}_\psi$  as follows:

$$|\psi_\pm\rangle = \frac{1}{\sqrt{2}} (|\psi_g\rangle \pm i |\psi_b\rangle) \quad (\text{B.11})$$

and with the eigenvalues of  $e^{\pm iE_{\text{eff}}}$ , respectively. We now express  $|\psi\rangle$  as the two eigenvectors as follows [[1](#)]:

$$|\psi\rangle = \frac{-i}{\sqrt{2}} (e^{i\lambda} |\psi_+\rangle - e^{-i\lambda} |\psi_-\rangle) \quad (\text{B.12})$$

We then see that

$$Q^t |\psi\rangle = \frac{-i}{\sqrt{2}} (e^{i(tE_{\text{eff}}+\lambda)} |\psi_+\rangle - e^{-i(tE_{\text{eff}}+\lambda)} |\psi_-\rangle) \quad (\text{B.13})$$

Upon projective measurement with  $P$ , we can then obtain

$$\begin{aligned} \langle \psi | Q^{-t} P Q^t | \psi \rangle &= \frac{1}{2} e^{i((tE_{\text{eff}}+\lambda)-(tE_{\text{eff}}+\lambda))} \langle \psi_+ | P | \psi_+ \rangle \\ &\quad - \frac{1}{2} e^{i((tE_{\text{eff}}+\lambda)-(-(tE_{\text{eff}}+\lambda)))} \langle \psi_- | P | \psi_+ \rangle \\ &\quad - \frac{1}{2} e^{i(-((tE_{\text{eff}}+\lambda)-(tE_{\text{eff}}+\lambda)))} \langle \psi_+ | P | \psi_- \rangle \\ &\quad + \frac{1}{2} e^{i(-(-(tE_{\text{eff}}+\lambda)-(-(tE_{\text{eff}}+\lambda)))} \langle \psi_- | P | \psi_- \rangle \\ &= \frac{1}{2} \langle \psi_+ | P | \psi_+ \rangle - \frac{1}{2} e^{i(t\Delta_{\text{eff}}+2\lambda)} \langle \psi_- | P | \psi_+ \rangle \\ &\quad - \frac{1}{2} e^{-i(t\Delta_{\text{eff}}+2\lambda)} \langle \psi_+ | P | \psi_- \rangle + \frac{1}{2} \langle \psi_- | P | \psi_- \rangle \quad (\text{B.14}) \end{aligned}$$

Then, calculating the four inner products, we obtain

$$\begin{aligned} \langle \psi_+ | P | \psi_+ \rangle &= \langle \psi_- | P | \psi_+ \rangle = \langle \psi_+ | P | \psi_- \rangle \\ &= \langle \psi_- | P | \psi_- \rangle = \frac{1}{2} \langle \psi_g | P | \psi_g \rangle = \frac{1}{2}. \quad (\text{B.15}) \end{aligned}$$

We thus obtain

$$\langle \psi | Q^{-t} P Q^t | \psi \rangle = \frac{1}{2} - \frac{1}{4} e^{i(t\Delta_{\text{eff}}+2\lambda)} - \frac{1}{4} e^{-i(t\Delta_{\text{eff}}+2\lambda)} \quad (\text{B.16})$$

Replacing the projective measurement with the observable  $O = \mathbb{I} - 2P$ , we obtain

$$\langle \psi | Q^{-t} O Q^t | \psi \rangle = \frac{1}{2} e^{i(t\Delta_{\text{eff}}+2\lambda)} + \frac{1}{2} e^{-i(t\Delta_{\text{eff}}+2\lambda)}. \quad (\text{B.17})$$

Similarly, if we use a Loschmidt-echo-like projective measurement, we would obtain Upon projective measurement with  $P$ , we can then obtain

$$\begin{aligned} \langle \psi | Q^{-t} | \psi \rangle \langle \psi | Q^t | \psi \rangle &= \frac{1}{2} \langle \psi_+ | \psi \rangle \langle \psi | \psi_+ \rangle - \frac{1}{2} e^{i(t\Delta_{\text{eff}}+2\lambda)} \langle \psi_- | \psi \rangle \langle \psi | \psi_+ \rangle \\ &\quad - \frac{1}{2} e^{-i(t\Delta_{\text{eff}}+2\lambda)} \langle \psi_+ | \psi \rangle \langle \psi | \psi_- \rangle + \frac{1}{2} \langle \psi_- | \psi \rangle \langle \psi | \psi_- \rangle \quad (\text{B.18}) \end{aligned}$$

Calculating the inner products, we obtain

$$\langle \psi_+ | \psi \rangle = \frac{-i}{\sqrt{2}} e^{i\lambda}, \quad \langle \psi_- | \psi \rangle = \frac{i}{\sqrt{2}} e^{-i\lambda}. \quad (\text{B.19})$$

Plugging in the results, we obtain

$$\langle \psi | Q^{-t} | \psi \rangle \langle \psi | Q^t | \psi \rangle = \frac{1}{2} + \frac{1}{4} e^{it\Delta_{\text{eff}}} + \frac{1}{4} e^{-it\Delta_{\text{eff}}}. \quad (\text{B.20})$$

Again replacing the projective measurement with the observable  $O' = 2|\psi\rangle\langle\psi| - \mathbb{I}$ , we obtain

$$\langle \psi | Q^{-t} (2|\psi\rangle\langle\psi| - \mathbb{I}) Q^t | \psi \rangle = \frac{1}{2} e^{it\Delta_{\text{eff}}} + \frac{1}{2} e^{-it\Delta_{\text{eff}}}. \quad (\text{B.21})$$

□

### Appendix C: Analytical properties of the periodic Gaussian

In this appendix, we establish several functional properties of the periodic Gaussian that are required for the analysis of our algorithms. In particular, we show that the periodic Gaussian satisfies strong convexity and smoothness conditions as shown in [Fig. 4](#). In our proofs in [Appendix D](#), we use the smoothness property to provide quadratic upper bounds and strong concavity to provide quadratic lower bounds for relevant regions.

We first define a simple Gaussian

$$\varphi_T(x) = \exp\left(-\frac{x^2 T^2}{2}\right). \quad (\text{C.1})$$

Based on this Gaussian, we define a periodic Gaussian

$$\Phi_T(x) = \frac{1}{\mathcal{Z}} \sum_{j \in \mathbb{Z}} \varphi_T(x + 2j\pi), \quad (\text{C.2})$$

where

$$\mathcal{Z} = \sum_{j \in \mathbb{Z}} \varphi_T(2j\pi) = \sum_{j \in \mathbb{Z}} \exp\left(-\frac{(2j\pi)^2 T^2}{2}\right), \quad (\text{C.3})$$

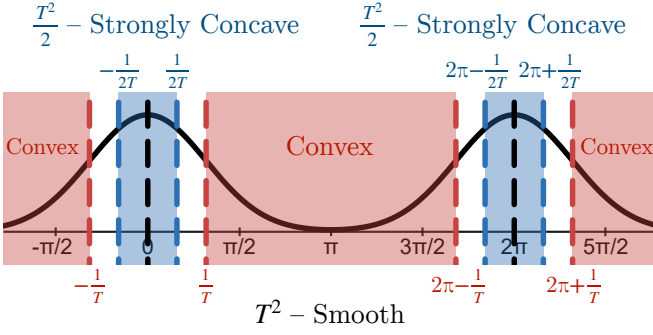


FIG. 4. *Regional functional properties of the periodic Gaussian.* In the periodic Gaussian with standard derivation  $T \geq 2/\pi$ , up to periodicity  $2\pi$ , the region  $[\frac{1}{T}, 2\pi - \frac{1}{T}]$  (red) is convex (Lemma C.1), the region  $[-\frac{1}{2T}, \frac{1}{2T}]$  (blue) is  $\frac{T^2}{2}$ -strongly concave (Lemma C.5), and the entire function is  $T^2$ -smooth (Lemma C.3).

such that  $\Phi_T(2j\pi) = 1$  for all  $j \in \mathbb{Z}$ . Note that  $\Phi_T(x)$  is the discrete-time Fourier/cosine transform of the discrete Gaussian

$$p_T(m) = \frac{1}{\sqrt{2\pi T \mathcal{Z}}} \exp\left(-\frac{m^2}{2T^2}\right) \quad (\text{C.4})$$

where

$$\begin{aligned} \Phi_T(k) &= \sum_{m=-\infty}^{\infty} p_T(m) \cos(km) \\ &= p_T(0) + 2 \sum_{m=1}^{\infty} p_T(m) \cos(km) \\ &= \frac{1}{\mathcal{Z}} \sum_{j \in \mathbb{Z}} \exp\left(-\frac{(k + 2j\pi)^2 T^2}{2}\right). \end{aligned} \quad (\text{C.5})$$

Thus, we can also find that

$$\mathcal{Z} = \sum_{m=-\infty}^{\infty} \frac{1}{\sqrt{2\pi T}} \exp\left(-\frac{m^2}{2T^2}\right). \quad (\text{C.6})$$

The following results are included for completeness and are used in the proofs of the main theorem in Appendix D. Readers interested only in the primary algorithmic contributions may skip forward to Appendix D.

### 1. Local convexity of the periodic Gaussian

We now provide some results on the convexity and smoothness of  $\Phi_T$  for the ease of proof in later sections. Due to periodicity, results that specify a range are applicable with a periodicity of  $2\pi$ . For example, when we say convexity holds for and interval  $[\frac{1}{T}, 2\pi - \frac{1}{T}]$ , the results also hold for  $[2j\pi + \frac{1}{T}, 2(j+1)\pi - \frac{1}{T}]$  for  $j \in \mathbb{Z}$ . To do so, we calculate the first four derivatives of  $\varphi_T$  as follows:

$$\varphi_T'(x) = -T^2 x \varphi_T(x), \quad (\text{C.7})$$

$$\varphi_T''(x) = (T^4 x^2 - T^2) \varphi_T(x), \quad (\text{C.8})$$

$$\varphi_T'''(x) = -T^4 x (T^2 x^2 - 3) \varphi_T(x), \quad (\text{C.9})$$

$$\varphi_T''''(x) = (T^8 x^4 - 6T^6 x^2 + 3T^4) \varphi_T(x). \quad (\text{C.10})$$

We first show a region of the periodic Gaussian that is convex, to both aid in the proof of later properties, and for the main proof.

**Lemma C.1** (Range of convexity of the periodic Gaussian). *Let  $T \geq 1/\pi$ . Then  $\Phi_T$  is convex on the interval  $[\frac{1}{T}, 2\pi - \frac{1}{T}]$ .*

*Proof.* From Eq. (C.8), we have  $\varphi_T''(x) = (T^4 x^2 - T^2) \varphi_T(x)$ . As  $\varphi_T(x) > 0$ , we can see that  $\varphi_T''(x) \geq 0$  if  $x \in \mathbb{R} \setminus [-\frac{1}{T}, \frac{1}{T}]$ , given that  $T^4 x^2 - T^2 \geq 0$ . As derivatives are linear transforms, we note that

$$\Phi_T''(x) = \frac{1}{\mathcal{Z}} \sum_{j \in \mathbb{Z}} \varphi_T''(x + 2j\pi). \quad (\text{C.11})$$

We can then see that if  $x \in [\frac{1}{T}, 2\pi - \frac{1}{T}]$ , then  $\varphi_T''(x + 2j\pi) \geq 0$  for all  $j \in \mathbb{Z}$ , hence  $\Phi_T''(x) \geq 0$ , then  $\Phi_T$  is convex.  $\square$

### 2. Smoothness of the periodic Gaussian

We now show the smoothness of the periodic Gaussian to provide quadratic upper bounds on the function.

**Definition C.1** (Smoothness of a function [92]). *Let  $f : \mathbb{R}^d \rightarrow \mathbb{R}$ , and  $\beta > 0$ . We say that  $f$  is  $\beta$ -smooth if it is differentiable and if  $\nabla f : \mathbb{R}^d \rightarrow \mathbb{R}^d$  is  $\beta$ -Lipschitz:*

$$\forall x, y \in \mathbb{R}^d, \|\nabla f(y) - \nabla f(x)\| \leq \beta \|y - x\|.$$

**Lemma C.2** (Properties of  $\beta$ -smooth functions [92]). *If  $f$  is  $\beta$ -smooth and convex, then for all  $x, y$ :*

$$f(y) \leq f(x) + \langle \nabla f(x), y - x \rangle + \frac{\beta}{2} \|y - x\|^2.$$

*Further, let  $\alpha \in [0, 1]$ , then for all  $x, y$*

$$\begin{aligned} \alpha f(x) + (1 - \alpha) f(y) - f(\alpha x + (1 - \alpha)y) \\ \leq \frac{\alpha(1 - \alpha)\beta}{2} \|y - x\|^2 \end{aligned}$$

**Lemma C.3** (Smoothness of the periodic Gaussian). *Let  $T \geq 2/\pi$ , then  $\Phi_T$  is  $T^2$ -smooth.*

*Proof.* From the definition of smoothness of a function and the Lipschitz property, we can find that the maximum value of the second derivative serves as a good  $\beta$ . Thus, the remainder of the proof is dedicated to bounding  $|\Phi_T''|$ . The high-level proof idea is to check critical points of  $\Phi_T''$  and provide upper bounds on their magnitude.

To find local maxima/minima in  $\Phi_T''$ , we find the roots for the third derivative  $\Phi_T'''$ , indicating the existence of

critical points, where again we can check by linearity of derivatives.

$$\Phi_T'''(x) = \frac{1}{Z} \sum_{j \in \mathbb{Z}} \varphi_T'''(x + 2j\pi). \quad (\text{C.12})$$

We first note that  $\varphi_T'''$  is an odd function such that  $\varphi_T'''(x) = -\varphi_T'''(-x)$ , hence  $x = 0$  is a critical point. Pairing  $\Phi_T'''(x + 2j\pi)$  and  $\Phi_T'''(x - 2(j+1)\pi)$  where  $j \in \mathbb{Z}_{\geq 0}$ , such that  $\Phi_T'''(x + 2j\pi) = -\Phi_T'''(x - 2(j+1)\pi)$ , we find that  $x = \pi$  is also a critical point.

We also observe that from the third and fourth derivative of  $\varphi(x)$  in Eqs. (C.9) and (C.10), we see that  $x = \frac{\sqrt{3}}{T}$  is a local maximum of  $\varphi_T''(x)$  in  $[\frac{1}{T}, \infty)$ . Plugging in  $T \geq 2/\pi$ , we can see that for all valid  $T$ ,  $\varphi(x)$  is monotonically decreasing for  $x \in [\frac{\sqrt{3}}{2}\pi, \infty)$ . In such ranges, we can use integrals to provide upper bounds.

*Case 1: Critical point at  $\Phi_T''(0)$ .*

Recall that

$$\Phi_T''(0) = \frac{1}{Z} \sum_{j \in \mathbb{Z}} \varphi_T''(2j\pi). \quad (\text{C.13})$$

Given that  $T \geq 2/\pi$ , for all  $j \in \mathbb{Z} \setminus \{0\}$ ,  $T^4(2\pi j)^2 - T^2 > 0$ , thus,  $\varphi_T''(2j\pi) > 0$ , while  $\varphi_T''(0) = -T^2$ . We now show that

$$\sum_{j \in \mathbb{Z} \setminus \{0\}} \varphi_T''(2j\pi) < T^2. \quad (\text{C.14})$$

Given that we can factorize out  $T^2$  from  $\varphi_T''(x)$ , we let  $\varrho_T(x) = T^{-2}\varphi_T''(x) = (T^2x^2 - 1)\varphi_T(x)$ . We then see that

$$\sum_{j \in \mathbb{Z} \setminus \{0\}} \varphi_T''(2j\pi) = 2 \sum_{j \in \mathbb{N}} \varphi_T''(2j\pi) = 2 \sum_{j \in \mathbb{N}} T^2 \varrho_T(x). \quad (\text{C.15})$$

Given the monotonically decreasing properties of  $\varphi_T''(2j\pi)$ , and by extension,  $\varrho_T(x)$ , we can upper bound the tail with an integral and find

$$\begin{aligned} \sum_{j \in \mathbb{N}} \varrho_T(2j\pi) &= \varrho_T(2\pi) + \sum_{j \in \mathbb{N} \setminus \{1\}} \varrho_T(2j\pi) \\ &= (4\pi^2 T^2 - 1)e^{-2\pi^2 T^2} + \sum_{j \in \mathbb{N} \setminus \{1\}} (4\pi^2 j^2 T^2 - 1)e^{-2j^2 \pi^2 T^2} \\ &\leq (4\pi^2 T^2 - 1)e^{-2\pi^2 T^2} + \int_{j=1}^{\infty} (4\pi^2 j^2 T^2 - 1)e^{-2j^2 \pi^2 T^2} \\ &= (4\pi^2 T^2 - 1)e^{-2\pi^2 T^2} + e^{-2\pi^2 T^2} = 4\pi^2 T^2 e^{-2\pi^2 T^2}, \end{aligned} \quad (\text{C.16})$$

and

$$\sum_{j \in \mathbb{N}} \varrho_T(2j\pi) \geq \int_{j=1}^{\infty} (4\pi^2 j^2 T^2 - 1)e^{-2j^2 \pi^2 T^2} = e^{-2\pi^2 T^2}. \quad (\text{C.17})$$

By the squeeze theorem, we find that

$$\lim_{T \rightarrow \infty} \sum_{j \in \mathbb{N}} \varrho_T(2j\pi) = 0 \quad (\text{C.18})$$

and by extension,

$$\lim_{T \rightarrow \infty} |\Phi_T(0)| = \frac{T^2}{Z} \leq T^2. \quad (\text{C.19})$$

On the other end, we want to check if the bounds also apply for all  $T \geq 2/\pi$ . Taking the derivative of  $4\pi^2 T^2 e^{-2\pi^2 T^2}$  over  $T$ , we find that the function is monotonically decreasing from  $T = \frac{1}{\sqrt{2}\pi}$ , so plugging in  $T = 2/\pi$ , we find

$$\sum_{j \in \mathbb{N}} \varrho_T(2j\pi) \leq \frac{16}{e^8} < 0.0055. \quad (\text{C.20})$$

Hence, we can find that

$$\sum_{j \in \mathbb{Z} \setminus \{0\}} \varphi_T''(2j\pi) \leq 0.0055 T^2, \quad (\text{C.21})$$

and by extension

$$\begin{aligned} |\Phi_T''(0)| &= \frac{1}{Z} \left| -T^2 + \sum_{j \in \mathbb{Z} \setminus \{0\}} \varphi_T''(2j\pi) \right| \\ &\leq \left| -T^2 + \sum_{j \in \mathbb{Z} \setminus \{0\}} \varphi_T''(2j\pi) \right| \leq T^2 \end{aligned} \quad (\text{C.22})$$

*Case 2: Critical point at  $\Phi_T''(\pi)$ .*

Given that  $x = \pi$  falls within  $[\frac{1}{T}, 2\pi - \frac{1}{T}]$ , as with the proof of Lemma C.1, we find that  $\varphi_T''(x + 2j\pi) \geq 0$  for all  $j \in \mathbb{Z}$ . Noting that  $\Phi_T''((2j+1)\pi) = \Phi_T''(-(2j+1)\pi)$ , we can find that

$$\Phi_T''(\pi) = \frac{1}{Z} \sum_{j \in \mathbb{Z}} \varphi_T''((2j+1)\pi) \leq 2 \sum_{j \in \mathbb{Z}_{\geq 0}} \varphi_T''((2j+1)\pi). \quad (\text{C.23})$$

Again letting  $\varrho_T(x) = T^{-2}\varphi_T''(x)$ , we can write the following:

$$\begin{aligned} \sum_{j \in \mathbb{Z}_{\geq 0}} \varrho_T''((2j+1)\pi) &= \varrho_T(\pi) + \sum_{j \in \mathbb{N}} \varrho_T((2j+1)\pi) \\ &\leq (\pi^2 T^2 - 1)e^{-\frac{\pi^2 T^2}{2}} + \int_{j=0.5}^{\infty} (4\pi^2 j^2 T^2 - 1)e^{-2j^2 \pi^2 T^2} \\ &= \frac{2\pi^2 T^2 - 1}{2e^{0.5\pi^2 T^2}} \end{aligned} \quad (\text{C.24})$$

Taking the derivative of the above over  $T$ , we find that the function is monotonically decreasing from  $T = \sqrt{\frac{5}{2}}\frac{1}{\pi}$ , so plugging in  $T = 2/\pi$ , we find

$$\sum_{j \in \mathbb{Z}_{\geq 0}} \varrho_T((2j+1)\pi) \leq \frac{7}{2e^2} < 0.475. \quad (\text{C.25})$$

Hence

$$\Phi_T''(\pi) < 0.95 T^2 < T^2. \quad (\text{C.26})$$

*Case 3: Additional critical points.*

Upon observing Eq. (C.9), we note that there are 3 roots of  $\varphi_T''(x)$ ,  $x = 0, \pm \frac{\sqrt{3}}{T}$ . This hints that there is a potential third case of critical points around  $x = \frac{\sqrt{3}}{T}$  and  $x = 2\pi - \frac{\sqrt{3}}{T}$  for  $\Phi_T''(x)$ . From Case 1, we know that  $\Phi''(0) < 0$ , and therefore must be a global minimum. (And  $\Phi''(2\pi) < 0$  for that matter.) Then, given that  $x = \pi$  is also a critical point and would not be a saddle point due to symmetry, if  $x = \pi$  is a local maximum, then the third set of critical points would be saddle points, and we need not worry. However, if  $x = \pi$  is a local minimum, then this set of critical points would then be local maxima.

We focus on the range where a possible local maximum can appear in  $x \in (0, \pi)$ . We can obtain the following:

$$\begin{aligned} \Phi_T''(x) &= \frac{1}{Z} \sum_{j \in \mathbb{Z}} \varphi_T''(x + 2j\pi) \\ &\leq T^2(\varrho_T(x) + \varrho_T(x - 2\pi)) \\ &\quad + T^2 \sum_{j \in \mathbb{N}} (\varrho_T(x + 2j\pi) + \varrho_T(x - 2(j+1)\pi)) \end{aligned} \quad (\text{C.27})$$

Factoring out the  $T^2$ , and from Eq. (C.20), we can bound

$$\begin{aligned} &(\varrho_T(x) + \varrho_T(x - 2\pi)) \\ &\quad + \sum_{j \in \mathbb{N}} (\varrho_T(x + 2j\pi) + \varrho_T(x - 2(j+1)\pi)) \\ &= (\varrho_T(x) + \varrho_T(2\pi - x)) \\ &\quad + \sum_{j \in \mathbb{N}} (\varrho_T(x + 2j\pi) + \varrho_T(2(j+1)\pi - x)) \\ &\leq 2\varrho_T\left(\frac{\sqrt{3}}{T}\right) + \sum_{j \in \mathbb{N}} 2\varrho_T(2j\pi) \\ &\leq \frac{4}{e^{1.5}} + \frac{32}{e^8} \leq 0.905 \end{aligned} \quad (\text{C.28})$$

Hence

$$\Phi_T''(\pi) < 0.905T^2 < T^2. \quad (\text{C.29})$$

□

### 3. Strongly concave areas of the periodic Gaussian

We now show the strong concavity in local regions of the periodic Gaussian to provide quadratic lower bounds of the function.

**Definition C.2** (Strong convexity of a function [92]). Let  $f : \mathbb{R}^d \rightarrow \mathbb{R}$ , and  $\mu > 0$ . We say that  $f$  is  $\mu$ -strongly convex if

$$\forall x, y \in \mathbb{R}^d, \langle \nabla f(y) - \nabla f(x), y - x \rangle \geq \mu \|y - x\|^2.$$

**Lemma C.4** (Properties of  $\mu$ -strongly convex functions [92]). *If and only if  $f$  is  $\mu$ -strongly convex, for all  $x$ ,*

$$g(x) = f(x) - \frac{\mu}{2} \|x\|^2$$

*is convex. For all  $x, y$ ,*

$$f(y) \geq f(x) + \langle \nabla f(x), y - x \rangle + \frac{\mu}{2} \|y - x\|^2.$$

*Further, let  $\alpha \in [0, 1]$ , then for all  $x, y$*

$$\begin{aligned} \alpha f(x) + (1 - \alpha)f(y) - f(\alpha x + (1 - \alpha)y) \\ \geq \frac{\alpha(1 - \alpha)\mu}{2} \|y - x\|^2 \end{aligned}$$

**Lemma C.5** (Range of convexity of the negated periodic Gaussian). *Let  $T \geq 2/\pi$ , then  $1 - \Phi_T$  is  $\frac{T^2}{2}$ -strongly convex on the interval  $[-\frac{1}{2T}, \frac{1}{2T}]$ .*

*Proof.* We want to show that on the interval  $[-\chi, \chi]$ ,  $1 - \Phi_T$  is  $\mu$ -strongly convex, and find values for  $\mu$  and  $\chi$  under the condition that  $T \geq 2/\pi$ .

To show  $\mu$  strong convexity for  $1 - \Phi_T$ , we show that  $1 - \Phi_T(x) - \frac{\mu}{2}x^2$  is convex. Taking the second derivative, we can see that we want to find a range of  $x$  and a value of  $\mu$  such that

$$-\Phi_T''(x) - \mu > 0 \Rightarrow -\Phi_T''(x) > \mu > 0. \quad (\text{C.30})$$

Thus, we now attempt to find a lower bound for  $-\Phi_T''(x)$  on the interval  $[-\chi, \chi]$ .

From Lemma C.1, we know that for  $x \in [\frac{1}{T}, 2\pi - T]$ ,  $-\Phi_T''(x) \leq 0$ . Hence, we require  $\chi < \frac{1}{T}$  to satisfy  $-\Phi_T''(\chi) > 0$ . For simplicity, we consider the case of  $\chi = \frac{1}{2T}$ .

We first show that  $\Phi_T''(x)$  is monotonically increasing in the range  $[0, \frac{1}{2T}]$ , which we show by proving  $\Phi_T'''(x) \geq 0$  in that region. By linearity, we once again see that

$$\begin{aligned} \Phi_T'''(x) &= \frac{1}{Z} \sum_{j \in \mathbb{Z}} \varphi_T'''(x + 2j\pi) \\ &= \frac{1}{Z} \left( \varphi_T'''(x) + \sum_{j \in \mathbb{N}} (\varphi_T'''(x + 2j\pi) + \varphi_T'''(x - 2j\pi)) \right). \end{aligned} \quad (\text{C.31})$$

First we see that  $\varphi_T'''(x) \geq 0$  when  $x \in [0, \frac{1}{2T}]$  by solving the inequality  $x(T^2x^2 - 3) \geq 0$ . Further, we note that from the fourth derivative  $\varphi_T''''(x)$ , we see that  $\varphi_T'''(x)$  is positive and monotonically increasing in  $(-\infty, -\frac{\sqrt{3+\sqrt{6}}}{T}]$  and thus  $(-\infty, -\frac{\sqrt{3+\sqrt{6}\pi}}{2}]$ . Thus, for all  $j$ , if  $x \in [0, \frac{1}{2T}]$ ,

$$\begin{aligned} \varphi_T'''(x + 2j\pi) + \varphi_T'''(x - 2j\pi) \\ = -\varphi_T'''(-x - 2j\pi) + \varphi_T'''(x - 2j\pi) \\ \geq -\varphi_T'''(-x - 2j\pi) + \varphi_T'''(-2j\pi) \geq 0. \end{aligned} \quad (\text{C.32})$$

$$\geq -\varphi_T'''(-x - 2j\pi) + \varphi_T'''(-2j\pi) \geq 0. \quad (\text{C.33})$$

We now show that for  $-\Phi_T''(\frac{1}{2T}) > \frac{T^2}{2}$ . Expanding the function, we obtain

$$-\Phi_T''\left(\frac{1}{2T}\right) = -\frac{1}{\mathcal{Z}}\varphi_T''\left(\frac{1}{2T}\right) - \frac{1}{\mathcal{Z}}\sum_{j \in \mathbb{N}}\varphi_T''\left(2j\pi + \frac{1}{2T}\right) - \frac{1}{\mathcal{Z}}\sum_{j \in \mathbb{N}}\varphi_T''\left(-2j\pi + \frac{1}{2T}\right) \quad (\text{C.34})$$

We first provide an upper bound for  $\mathcal{Z}$ . Recall that

$$\begin{aligned} \mathcal{Z} &= \sum_{j \in \mathbb{Z}} \varphi_T(2j\pi) = 1 + 2\varphi_T(2\pi) + 2 \sum_{j \in \mathbb{N} \setminus \{1\}} \varphi_T(2\pi j) \\ &\leq 1 + 2e^{-2\pi^2 T^2} + 2 \int_{j=1}^{\infty} e^{-2\pi^2 j^2 T^2} \\ &< 1 + 2e^{-2\pi^2 T^2} + 2\sqrt{\frac{\pi}{2}} e^{-4\pi^2 T^2} \\ &\leq 1 + 2e^{-8} + 2\sqrt{\frac{\pi}{2}} e^{-16} < 1.007. \end{aligned} \quad (\text{C.35})$$

Then, we see that

$$-\varphi_T''\left(\frac{1}{2T}\right) = \frac{3T^2}{4e^{0.125}} > 0.66T^2 \quad (\text{C.36})$$

Next, as we know that  $\frac{1}{\mathcal{Z}}\sum_{j \in \mathbb{N}}\varphi_T''(2j\pi + \frac{1}{2T})$  is positive, so we can upper bound this by

$$\sum_{j \in \mathbb{N}} \varphi_T''\left(2j\pi + \frac{1}{2T}\right) \leq \sum_{j \in \mathbb{N}} \varphi_T''(2j\pi). \quad (\text{C.37})$$

We know by Eq. (C.20) that

$$\sum_{j \in \mathbb{N}} \varphi_T''(2j\pi) = T^2 \sum_{j \in \mathbb{N}} \varrho_T(2j\pi) \leq \frac{16T^2}{e^8} < 0.0055T^2. \quad (\text{C.38})$$

On the other side, we can bound

$$\begin{aligned} \sum_{j \in \mathbb{N}} \varphi_T''\left(-2j\pi + \frac{1}{2T}\right) &= \sum_{j \in \mathbb{N}} \varphi_T''\left(2j\pi - \frac{1}{2T}\right) \\ &\leq \sum_{j \in \mathbb{N}} \varphi_T''((2j - 0.25)\pi) \leq T^2 \sum_{j \in \mathbb{N}} \varrho_T''((2j - 0.25)\pi) \end{aligned} \quad (\text{C.39})$$

Hence, we can then bound

$$\begin{aligned} &\sum_{j \in \mathbb{N}} \varrho_T''((2j - 0.25)\pi) \\ &\leq \varrho_T''\left(\frac{7}{4}\pi\right) + \int_{j=0.875}^{\infty} (4\pi^2 j^2 T^2 - 1) e^{-2j^2 \pi^2 T^2} \\ &= \frac{49\pi^2 T^2 + 13}{16} e^{-\frac{49\pi^2 T^2}{32}} \end{aligned} \quad (\text{C.40})$$

Differentiating the above by  $T$ , we find that the function is monotonically decreasing from  $T = \frac{\sqrt{19}}{7\pi} < \frac{2}{\pi}$ . Hence,

the maximum in our range can be found at  $T = \frac{2}{\pi}$ , and we bound

$$\frac{49\pi^2 T^2 + 13}{16} e^{-\frac{49\pi^2 T^2}{32}} \leq \frac{209}{16e^{6.125}} < 0.03 \quad (\text{C.41})$$

Thus, overall, we obtain

$$-\Phi_T''\left(\frac{1}{2T}\right) > \frac{0.66 - 0.0055 - 0.03}{1.007} T^2 > 0.62T^2 > \frac{T^2}{2} \quad (\text{C.42})$$

□

## Appendix D: Further details on GLSAE

We feature a mixture of ideas from Gaussian filtering to implement amplitude estimation. Gaussian filtering was previously discussed in the context of amplitude estimation by Yang and Yang [11], but the filter function is computed purely on classical computers and does not apply importance sampling of quantum circuit executions, and thus does not reach Heisenberg-limited scaling. Here we combine ideas from Gaussian-filtered phase estimation protocols [19–21] to provide Gaussian Least Squares Amplitude Estimation (GLSAE), a simplified algorithm that shows the achievement of Heisenberg-limited runtimes as well as limited low-depth circuit guarantees.

### 1. Algorithm and discussions for GLSAE

Our algorithm follows a simple three-step protocol:

1. Sample iteration counts  $m$  from a sampling filter function.
2. Apply amplitude amplification circuits corresponding to the sampled iteration  $m$  and obtain measurement outcome  $Z_m$ .
3. Minimize a loss function  $\bar{\mathcal{L}}$  to find the underlying eigengap  $\Delta_{\text{eff}} = 4\lambda$  and use  $\lambda$  to obtain the outcome  $a = \sin^2(\lambda)$ .

To find the appropriate sampling filter function, we require an even discrete function, as the estimates of the signal  $S(m)$  are only accessible when  $m$  is a positive integer, and a function that decays as  $m$  grows, such that we can truncate the cases where  $m$  is larger, and limit the length of the circuit. A suitable candidate, as noted by Ding *et al.* [21], is the discrete Gaussian established in Appendix C as follows:

$$p_T(m) = \frac{1}{\sqrt{2\pi T \mathcal{Z}}} \exp\left(-\frac{m^2}{2T^2}\right) \quad (\text{D.1})$$

where  $\mathcal{Z} = \sum_{m=-\infty}^{\infty} \frac{1}{\sqrt{2\pi T}} \exp\left(-\frac{m^2}{2T^2}\right)$ . This serves as the probability distribution for sampling the evolution iteration  $m$  for the amplitude amplification circuit. Recall

---

**Algorithm 1:** Gaussian Least Square Amplitude Estimation (GLSAE)

---

**Input:** State  $|\psi\rangle$ , Projector  $P$ , Walk operator  $Q$ , Gaussian width  $T$ , Maximum circuit depth  $M$ , Number of parallel queries  $N$ , Precision  $\epsilon$

**Output:** Estimate of  $a = \|P|\psi\rangle\|^2$

- 1 Sample  $N$  iterations  $m$  from truncated discrete Gaussian

$$\tilde{p}_T(m) = \begin{cases} \frac{1}{\sqrt{2\pi T^2}} \exp\left(-\frac{m^2}{2T^2}\right) & 1 \leq |m| \leq M \\ 0 & |m| > M \\ 1 - \sum_{\tau \neq 0} \tilde{p}_T(\tau) & m = 0 \end{cases}$$

- 2 **for** each sampled  $m$  out of  $N$  samples **do**

- 3   **if**  $|m| = 2t + 1$ ,  $t \in \mathbb{Z}_{\geq 0}$  **then**
- 4    | Measure observable  $\mathbb{I} - 2P$  on state  $Q^t|\psi\rangle$  and obtain  $Z_m \in \{\pm 1\}$
- 5   **else if**  $|m| = 2t$ ,  $t \in \mathbb{N}$  **then**
- 6    | Measure observable  $2|\psi\rangle\langle\psi| - \mathbb{I}$  on state  $(\mathbb{I} - 2P)Q^{t-1}|\psi\rangle$  and obtain  $Z_m \in \{\pm 1\}$

- 7 Obtain estimate  $\tilde{\lambda}$  of  $\lambda$  from

$$\begin{aligned} \tilde{\lambda} &= \arg \min_{\theta \in [0, \frac{\pi}{2}]} \tilde{\mathcal{L}}(\theta) \\ &= \arg \min_{\theta \in [0, \frac{\pi}{2}]} \frac{1}{N} \sum_{m \sim \tilde{p}_T} (Z_m - \cos(2\theta m))^2 \end{aligned}$$

via a two-level grid search for  $\chi^*$  across

$$\theta \in \left\{ \frac{\pi\chi}{2M} : \chi \in [M] \right\}$$

followed by a more fine-grained search for  $\eta^*$  across

$$\theta \in \left\{ \frac{\pi\chi^*}{2M} + \frac{\eta\epsilon}{2} : \eta \in \left[ -\frac{8\pi}{M\epsilon}, \frac{8\pi}{M\epsilon} \right] \right\}$$

- 8 **return**  $\tilde{a} = \sin^2(\tilde{\lambda})$  up to additive precision  $\epsilon$
- 

that the discrete-time cosine transform [33] of the  $p_T$  is then

$$\begin{aligned} \Phi_T(k) &= \sum_{m=-\infty}^{\infty} p_T(m) \cos(km) \\ &= \frac{1}{Z} \sum_{j \in \mathbb{Z}} \exp\left(-\frac{(k + 2j\pi)^2 T^2}{2}\right). \end{aligned} \quad (\text{D.2})$$

In practice, we generate the discrete Gaussian by approximating  $\mathcal{Z}$  with  $\tilde{\mathcal{Z}} = \sum_{m=-\rho T}^{\rho T} \frac{1}{\sqrt{2\pi T}} \exp\left(-\frac{m^2}{2T^2}\right)$  and apply a truncated version of the discrete Gaussian where

$$\tilde{p}_T(m) = \begin{cases} \frac{1}{\sqrt{2\pi T^2}} \exp\left(-\frac{m^2}{2T^2}\right) & 1 \leq |m| \leq \sigma T \\ 0 & |m| > \sigma T \\ 1 - \sum_{\tau \neq 0} \tilde{p}_T(\tau) & m = 0 \end{cases} \quad (\text{D.3})$$

with  $\sigma \leq \rho$  to limit the maximum length at  $M = \lceil \sigma T \rceil$  and approaching the Heisenberg limit.

We then sample the output of amplitude amplification circuits with the number of walk operators applied based on the truncated Gaussian prior distribution constructed above. As mentioned in the main text, for cases when  $m = 2t + 1$  is odd, we use the standard amplitude amplification circuit where we apply  $t$  iterations of the walk operator  $Q$  and measure with  $\mathbb{I} - 2P$ . When  $m = 2t$  is even, we use the Loschmidt-echo-esque circuit and apply  $t - 1$  iterations of the walk operator  $Q$ , followed by an additional  $\mathbb{I} - 2P$  and measure with  $2|\psi\rangle\langle\psi| - \mathbb{I}$ . Given that the signals that we collect here are cosine, we have  $S(m) = S(-m)$ , thus, if negative  $m$  is sampled, we simply ignore the negative sign, and set  $Z_{-m} = Z_m$ .

Inspired by Ding and Lin [17, 20], for a given  $N$  samples with their evolution iterations  $\{m, Z_m\}$  where  $\mathbb{E}[Z_m|m] = \cos(2\lambda m)$ , we minimize the mean square error loss function of the measured result and its cosine signal over samples from the truncated discrete Gaussian  $p_T$

$$\tilde{\mathcal{L}}(\theta) = \frac{1}{N} \sum_{m \sim \tilde{p}_T} (Z_m - \cos(2\theta m))^2 \quad (\text{D.4})$$

by performing a two-level grid search across  $\chi \in [M]$  such that  $\theta = \frac{\pi\chi}{2M} \in [0, \pi/2]$  followed by a more fine grained search in  $\eta$  with precision  $\kappa = \frac{\epsilon}{2}$  over  $[\frac{\pi\chi}{2M} - \frac{4\pi}{M}, \frac{\pi\chi}{2M} + \frac{4\pi}{M}]$ . A similar two-level search approach can be found in the code implementation of Ding *et al.* [21]. The algorithm is summarized in Algorithm 1.

As we can utilize statistical phase estimation algorithms to obtain energy differences that encode the results for amplitude estimation, we should be able to, in principle, obtain the low-depth amplitude estimation by executing low-depth phase estimation algorithms [20, 21]. We expect such algorithms to then obtain a trade-off between the maximum circuit depth  $M$  and the number of total circuit samples  $N$ , which has the invariance of  $M^2 N \in \tilde{O}(\epsilon^{-2})$  in both phase estimation [93–95] and amplitude estimation [34, 35].<sup>1</sup> However, when applying such statistical phase estimation algorithms directly to amplitude estimation, some complications arise.

Our loss function operates as a least squares estimator that guarantees that, given enough samples, a minimum can be found around  $\theta = \lambda$  without major distortions. If we replace  $Z_m$  with its expected value  $\mathbb{E}[Z_m|m] = \cos(2\lambda m)$ , we can indeed see that we minimize  $(\cos(2\lambda m) - \cos(2\theta m))^2$  over  $N$  samples. However, given we only have access to the cosine signals, we find that the minimum would be found at not only  $\theta = \lambda$ , but also  $\theta = -\lambda$ . Considering the loss function as a combination of two periodic Gaussians with peaks at  $\theta - \lambda$  and

<sup>1</sup> In prior literature for low-depth amplitude estimation [12, 13], this invariance is often phrased as  $\mathcal{DN} \in \tilde{O}(\epsilon^{-2})$ , where  $\mathcal{D}$  is the maximum depth, and  $\mathcal{N}$  is the total number of queries to the state preparation unitary, and as such, is more often phrased as a *depth-query invariance*.

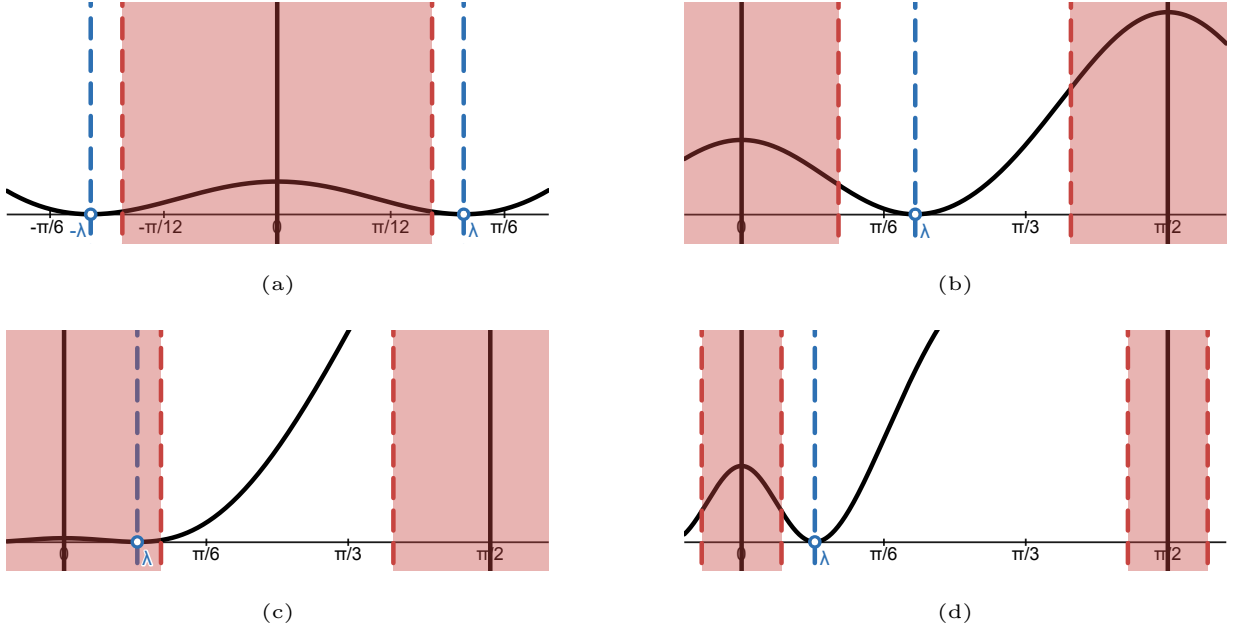


FIG. 5. *Failure regions for GLSAE.* We draft the ideal loss function for GLSAE without the measurement errors to show why GLSAE fails in regions close to 0 and  $\pi/2$ . In panel (a), we see that when plotted, the ideal loss function (black solid line) has symmetric minima at  $\theta = \pm\lambda$  (blue dashed lines) formed from overlapping Gaussian peaks from the periodic Gaussians. In low depth situations, when the standard deviation  $T$  of the discrete Gaussian is small, the minimum can still be found when  $\lambda$  is far from either 0 or  $\pi/2$  as shown in panel (b). However, when  $\lambda$  is close to either 0 or  $\pi/2$  (in the red shaded area), the minimum is not easy to discern, and worse so under noise. When the standard deviation  $T$  of the discrete Gaussian is high enough, then the overlap can be reduced, and the invalid region (red shaded area) shrinks, such that we can still discern the peak even under noise, as known in panel (d).

$\theta + \lambda$  when we factor in the discrete Gaussian sampling, we can see that we would have trouble discerning the two peaks when  $\lambda$  is close to zero. At the Heisenberg limit,  $T$  is large, and the two Gaussians are still sharp enough to discern between the two, but as we approach low-depth circuits, these two peaks become harder to discern, and GLSAE fails. The same applies to cases where  $\lambda$  is close to  $\pi/2$ , and we have two peaks at  $\theta = \lambda$  and  $\theta = \pi - \lambda$ . Fig. 5 shows such discussions when plotted. As a consequence, the range of  $a$  that can be estimated is limited by the width of the Gaussian peak, as parameterized by  $T$  and limited by the maximum circuit depth  $M = \lceil \sigma T \rceil$ . This limitation of the inability to estimate amplitudes  $a$  close to 0 or 1 is not unique to our algorithm, but has also been shown to exist in prior work [8].

## 2. Proofs for GLSAE

We now discuss the proof for GLSAE. We define the loss function

$$\mathcal{L}_m(\theta) = (Z_m - \cos(2\theta m))^2, \quad (\text{D.5})$$

where the total empirical loss can be defined as

$$\tilde{\mathcal{L}}(\theta) = \frac{1}{N} \sum_{m \sim \tilde{p}_T} (Z_m - \cos(2\theta m))^2. \quad (\text{D.6})$$

In an abuse of notation, we drop the subscript for  $\mathcal{L}_m$  when  $m$  is arbitrary, e.g., when  $\mathcal{L}_m$  is wrapped in an expected value. Calculating the expected value of the loss, we obtain

$$\begin{aligned} \mathbb{E}[\mathcal{L}(\theta)] &= \mathbb{E}[(Z_m - \cos(2\theta m))^2] \\ &= \mathbb{E}[Z_m^2] - 2\mathbb{E}[Z_m \cos(2\theta m)] + \mathbb{E}[\cos^2(2\theta m)] \\ &= 1 - 2\mathbb{E}[\cos(2\lambda m) \cos(2\theta m)] + \mathbb{E}[\cos^2(2\theta m)] \\ &= \frac{3}{2} - \mathbb{E}[\cos(2(\theta - \lambda)m)] - \mathbb{E}[\cos(2(\theta + \lambda)m)] \\ &\quad + \frac{1}{2}\mathbb{E}[\cos(4\theta m)]. \end{aligned} \quad (\text{D.7})$$

where the second-to-last equality is obtained by observing  $\mathbb{E}[Z_m^2] = 1$  due to  $Z_m = \pm 1$ , as well as  $\mathbb{E}[Z_m | m] = \cos(2\lambda m)$ , and the last equality is obtained by expressing a product of cosines as a sum of cosines.

We now define an ideal error function  $\mathcal{E}$  where the signal  $\cos(2\lambda m)$  of a given time point is provided without sampling or noise, and no truncation is performed on the discrete Gaussian. In this case, the sampling probability takes the form of Eq. (C.4). We then obtain the following:

$$\mathcal{E}(\theta) = \sum_{m=-\infty}^{\infty} p_T(m) (\cos(2\lambda m) - \cos(2\theta m))^2$$

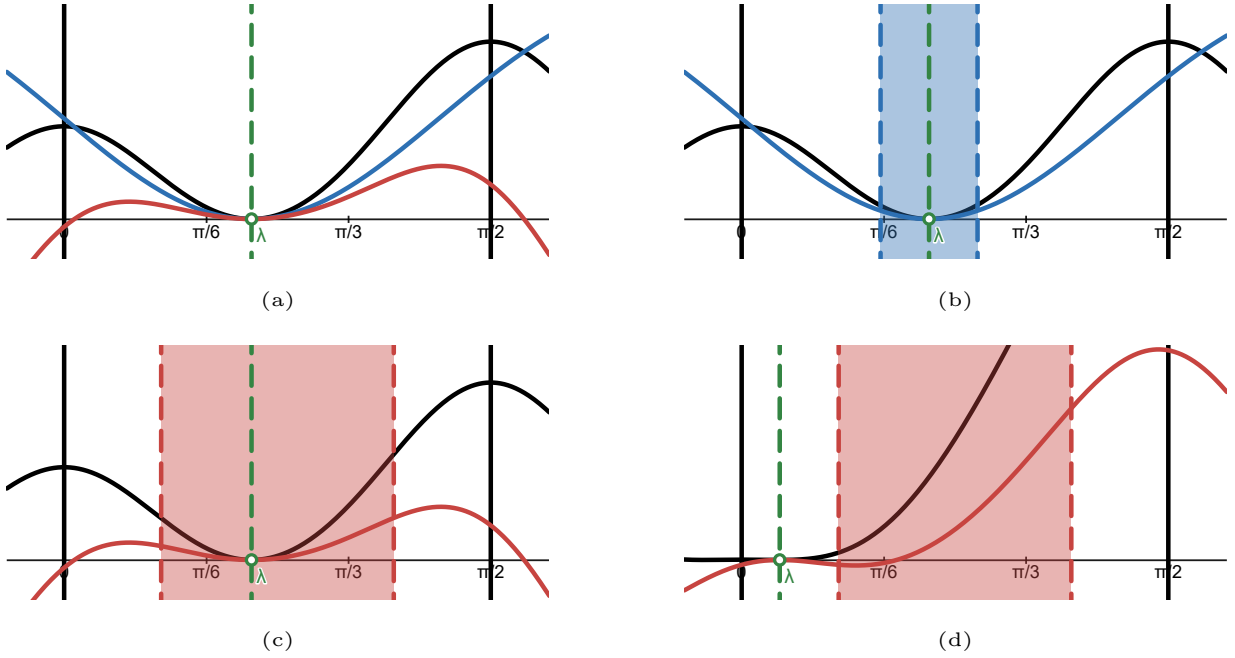


FIG. 6. *Analysis of the loss function failure region.* We illustrate the decomposition of the ideal loss function for GLSAE without the measurement errors to show how to quantify the regions where GLSAE fails. In panel (a), we decompose the ideal error function  $\mathcal{E}(\theta)$  (black) as a sum of a negated periodic Gaussian  $\mathcal{E}_1(\theta)$  (blue) and an indicator function  $\mathcal{E}_2(\theta)$  (red) of the convexity of  $\Phi_T$ . In the blue shaded region of panel (b), strong convexity of  $\mathcal{E}_1(\theta)$  can be found and used to provide quadratic lower bounds on  $\mathcal{E}_1(\theta)$ . In panel (c), the red shaded area indicates the range where  $\Phi_T(4\theta)$  is convex, and hence the quadratic lower bounds hold for  $\mathcal{E}(\theta)$  and the minimum is easily discernible. In panel (d),  $\lambda$  is outside of the red shaded area where  $\mathcal{E}_2(\theta) < 0$ , thus the quadratic lower bounds for  $\mathcal{E}(\theta)$  may not hold. In this case, the minimum is not easily discernible, more so after noise is added.

$$\begin{aligned}
&= \sum_{m=-\infty}^{\infty} p_T(m) \left( 1 + \frac{1}{2} \cos(4\lambda m) - \cos(2(\theta - \lambda)m) \right. \\
&\quad \left. - \cos(2(\theta + \lambda)m) + \frac{1}{2} \cos(4\theta m) \right) \\
&= 1 + \frac{\Phi_T(4\lambda)}{2} - \Phi_T(2(\theta - \lambda)) - \Phi_T(2(\theta + \lambda)) + \frac{\Phi_T(4\theta)}{2} \quad (\text{D.8})
\end{aligned}$$

The main proof idea is to use the smoothness and convexity properties shown in [Appendix C](#) to provide upper and lower quadratic bounds. We can decompose  $\mathcal{E}(\theta)$  into two terms

$$\begin{aligned}
\mathcal{E}_1(\theta) &= 1 - \Phi_T(2(\theta - \lambda)) \\
\mathcal{E}_2(\theta) &= \frac{\Phi_T(4\lambda)}{2} - \Phi_T(2(\theta + \lambda)) + \frac{\Phi_T(4\theta)}{2}, \quad (\text{D.9})
\end{aligned}$$

where we observe that  $\mathcal{E}_1(\theta)$  is a negated periodic Gaussian centered at  $2(\theta - \lambda)$  and  $\mathcal{E}_2(\theta)$  is an indicator of the convexity of  $\Phi_T$  in the range  $[2 \min(\theta, \lambda), 2 \max(\theta, \lambda)]$ . Note that the minimum of  $\mathcal{E}_1(\theta)$  occurs when  $\theta = \lambda$  up to periodicity  $\pi$  of  $\theta$  and is the solution we are looking for, and where we can apply smoothness and strong convexity arguments to provide quadratic upper and lower bounds.

However, since we can only access a noisy version of  $\mathcal{E}(\theta)$  without isolating  $\mathcal{E}_1(\theta)$ , to ensure that the quadratic bounds of  $\mathcal{E}_1(\theta)$  also hold for  $\mathcal{E}(\theta)$ , we should have  $\mathcal{E}_2(\theta) >$

0, or where  $\Phi_T$  is convex. Per [Lemma C.1](#), we know that said range occurs when  $\theta \in [\frac{1}{4T}, \frac{\pi}{2} - \frac{1}{4T}]$ . Thus, in the range of  $\theta \in [0, \frac{1}{4T}] \cup [\frac{\pi}{2} - \frac{1}{4T}, \frac{\pi}{2}]$ ,  $\mathcal{E}_2(\theta) < 0$  and the quadratic bounds no longer hold for  $\mathcal{E}(\theta)$ . We illustrate this in [Fig. 6](#).

#### a. Truncation and sampling errors of the loss function

Before providing the main proof using the quadratic bounds as mentioned, we need to consider the effects of both the truncation error and the sampling error. We further define

$$\begin{aligned}
\mathcal{F}(\theta) &= \mathcal{E}(\theta) + \frac{1}{2} - \frac{\Phi_T(4\lambda)}{2} \\
&= \frac{3}{2} - \Phi_T(2(\theta - \lambda)) - \Phi_T(2(\theta + \lambda)) + \frac{\Phi_T(4\theta)}{2} \quad (\text{D.10})
\end{aligned}$$

so that the terms correspond to  $\mathbb{E}[\mathcal{L}(\theta)]$ .

We now provide bounds on the error caused by the truncation of the discrete Gaussian  $\tilde{p}_T$  from [Eq. \(D.3\)](#) similar to Refs. [\[21, 96\]](#).

**Lemma D.1** (Truncation error of the loss from the discrete Gaussian). *Given  $\delta > 0$ , if  $\sigma \in \Omega(\log^{\frac{1}{2}}(\frac{1}{\delta}))$  and  $\rho \geq \sigma$ , we have*

$$|\mathbb{E}[\mathcal{L}(\theta)] - \mathcal{F}(\theta)| \leq \delta^2 \quad (\text{D.11})$$

*Proof.* We wish to find the truncation errors caused by two truncations: the first being the truncation error from truncating Gaussian samples, and the second from obtaining the normalization coefficient via a truncated sum.

From the triangle inequality, we can find that

$$\begin{aligned} |\mathbb{E}[\mathcal{L}(\theta)] - \mathcal{F}(\theta)| &\leq |\mathbb{E}[\cos(2(\theta - \lambda)m)] - \Phi(2(\theta - \lambda))| \\ &\quad + |\mathbb{E}[\cos(2(\theta + \lambda)m)] - \Phi(2(\theta + \lambda))| \\ &\quad + \frac{1}{2} |\mathbb{E}[\cos(4\theta m)] - \Phi(4\theta)| \end{aligned} \quad (\text{D.12})$$

Given that the above 3 terms have the same structure, we assume a general  $\gamma$  where we find

$$\begin{aligned} &\mathbb{E}_{m \sim \tilde{p}_T} [\cos(\gamma m)] \\ &= \sum_{|m| \leq \sigma T} \tilde{p}_T(m) \cos(\gamma m) \\ &= \sum_{|m| \leq \sigma T} \frac{\mathcal{Z}}{\tilde{\mathcal{Z}}} p_T(m) \cos(\gamma m) + \left(1 - \sum_{|m| \leq \sigma T} \frac{\mathcal{Z}}{\tilde{\mathcal{Z}}} p_T(m)\right) \\ &= \sum_{|m| \leq \sigma T} \frac{\mathcal{Z}}{\tilde{\mathcal{Z}}} p_T(m) \cos(\gamma m) \\ &\quad + \left( \frac{\tilde{\mathcal{Z}} - \mathcal{Z}}{\tilde{\mathcal{Z}}} + \sum_{|m| > \sigma T} \frac{\mathcal{Z}}{\tilde{\mathcal{Z}}} p_T(m) \right). \end{aligned} \quad (\text{D.13})$$

We can then observe that

$$\begin{aligned} &|\mathbb{E}[\cos(\gamma m)] - \Phi_T(\gamma)| \\ &= \left| \sum_{|m| \leq \sigma T} \tilde{p}_T(m) \cos(\gamma m) - \sum_{m=-\infty}^{\infty} p_T(m) \cos(\gamma m) \right| \\ &\leq \left| \frac{\mathcal{Z} - \tilde{\mathcal{Z}}}{\tilde{\mathcal{Z}}} \sum_{m=-\infty}^{\infty} p_T(m) \cos(\gamma m) + \frac{\tilde{\mathcal{Z}} - \mathcal{Z}}{\tilde{\mathcal{Z}}} \right. \\ &\quad \left. + \sum_{|m| > \sigma T} \frac{\mathcal{Z}}{\tilde{\mathcal{Z}}} p_T(m) (1 - \cos(\gamma m)) \right| \\ &\leq \left| \frac{\mathcal{Z} - \tilde{\mathcal{Z}}}{\tilde{\mathcal{Z}}} (\Phi_T(\gamma) - 1) \right| + \sum_{|m| > \sigma T} \left| \frac{\mathcal{Z}}{\tilde{\mathcal{Z}}} p_T(m) (1 - \cos(\gamma m)) \right| \\ &\leq \left| \frac{\mathcal{Z} - \tilde{\mathcal{Z}}}{\tilde{\mathcal{Z}}} \right| + 2 \sum_{|m| > \sigma T} \frac{\mathcal{Z}}{\tilde{\mathcal{Z}}} p_T(m). \end{aligned} \quad (\text{D.14})$$

Giving us the truncation error from truncating Gaussian samples as the second term, and the truncation in estimating the normalization coefficient as the first term. The second term can be further upper-bounded by showing that

$$\begin{aligned} \sum_{|m| > \sigma T} \frac{\mathcal{Z}}{\tilde{\mathcal{Z}}} p_T(m) &= \sum_{|m| > \sigma T} \frac{1}{\sqrt{2\pi T \tilde{\mathcal{Z}}}} e^{-\frac{m^2}{2T^2}} \\ &\leq \sum_{|m| > \sigma T} \frac{1}{\sqrt{2\pi T}} e^{-\frac{m^2}{2T^2}} \end{aligned}$$

$$\begin{aligned} &\leq 2 \int_{m=\sigma T}^{\infty} \frac{1}{\sqrt{2\pi T}} e^{-\frac{m^2}{2T^2}} dt \\ &= \int_{s=\sigma}^{\infty} \sqrt{\frac{2}{\pi}} e^{-\frac{s^2}{2}} ds \leq e^{-\sigma^2} \leq \frac{2\delta^2}{15} \end{aligned} \quad (\text{D.15})$$

Similar to the above, the first term can be bounded as follows:

$$\frac{\mathcal{Z} - \tilde{\mathcal{Z}}}{\tilde{\mathcal{Z}}} = \sum_{|m| > \rho T} \frac{1}{\sqrt{2\pi T \tilde{\mathcal{Z}}}} e^{-\frac{m^2}{2T^2}} \leq e^{-\rho^2} \leq e^{-\sigma^2} \leq \frac{2\delta^2}{15}. \quad (\text{D.16})$$

Thus, for all  $\gamma$ , we can obtain

$$|\mathbb{E}[\cos(\gamma m)] - \Phi(\theta)| \leq \frac{2\delta^2}{5}, \quad (\text{D.17})$$

and hence

$$|\mathbb{E}[\mathcal{L}(\theta)] - \mathcal{F}(\theta)| \leq \delta^2. \quad (\text{D.18})$$

□

We now obtain bounds regarding the number of samples  $N$  via the Hoeffding bound of the difference of losses similar to Refs. [21, 96]. Let

$$\mathcal{D}_m(\theta, \lambda) = \mathcal{L}_m(\theta) - \mathcal{L}_m(\lambda). \quad (\text{D.19})$$

We then obtain the following lemma.

**Lemma D.2** (Sampling error from measurements). *Let  $0 \leq \xi \leq 1$ ,  $\delta \geq 0$ ,  $\lambda \in [0, \frac{\pi}{2}]$  and  $\kappa > 0$ . We define a grid  $G$  in range  $[0, \frac{\pi}{2}]$  with spacing  $\kappa$  and let  $J = \lfloor \frac{\pi}{2\kappa} \rfloor$  such that  $G = \{\frac{k}{\kappa} : k \in [J] \cup \{0\}\}$ . For all possible values of  $\theta \in G$ , if  $N \in \mathcal{O}(\frac{1}{\delta^2} \log(\frac{1}{\kappa\xi}))$ , then*

$$\Pr \left[ \left| \frac{1}{N} \sum_m (\mathcal{D}_m(\theta, \lambda)) - \mathbb{E}[\mathcal{D}(\theta, \lambda)] \right| \leq \sigma T \delta |\theta - \lambda| \right] \geq 1 - \xi.$$

*Proof.* Expanding the difference of losses, we obtain

$$\begin{aligned} \mathcal{D}_m(\theta, \lambda) &= \mathcal{L}_m(\theta) - \mathcal{L}_m(\lambda) \\ &= (1 - 2Z_m \cos(2\theta m) + \cos^2(2\theta m)) \\ &\quad - (1 - 2Z_m \cos(2\lambda m) + \cos^2(2\lambda m)) \\ &= \cos^2(2\theta m) - \cos^2(2\lambda m) \\ &\quad + 2Z_m \cos(2\lambda m) - 2Z_m \cos(2\theta m) \\ &= (\cos(2\theta m) + \cos(2\lambda m) - 2Z_m) \\ &\quad \times (\cos(2\theta m) - \cos(2\lambda m)) \end{aligned} \quad (\text{D.20})$$

Noting the inequality  $|\cos(2\theta m) + \cos(2\lambda m) - 2Z_m| \leq 4$  and the Lipschitz property, we obtain the following:

$$\begin{aligned} |\mathcal{D}_m(\theta, \lambda)| &\leq 4(\cos(2\lambda m) - \cos(2\theta m)) \\ &\leq 4 \left| \max_{\phi} \frac{\partial \cos(2\phi m)}{\partial \phi} \right| |\theta - \lambda| \end{aligned}$$

$$\begin{aligned} &\leq 8m \left| \max_{\phi} \sin(2\phi m) \right| |\theta - \lambda| \\ &\leq 8\sigma T |\theta - \lambda| \end{aligned} \quad (\text{D.21})$$

where the last inequality is obtained by noting that for all  $m$ ,  $m \leq \sigma T$ . From this bound, we note that  $\mathcal{D}_m(\theta, \lambda) \in [-8\sigma T|\theta - \lambda|, 8\sigma T|\theta - \lambda|]$ , which we can use as the bounds for Hoeffding's inequality, where we can obtain

$$\begin{aligned} \Pr \left[ \left| \frac{1}{N} \sum_m (\mathcal{D}_m(\theta, \lambda)) - \mathbb{E}[\mathcal{D}(\theta, \lambda)] \right| \geq \eta \right] \\ \leq \exp \left( -\frac{2N\eta^2}{(16\sigma T|\theta - \lambda|)^2} \right). \end{aligned} \quad (\text{D.22})$$

We note that  $|G| = J+1 = \lfloor \frac{\pi}{2\kappa} \rfloor + 1$ , thus by union bound for  $\theta \in G$ ,

$$\begin{aligned} \Pr \left[ \bigcup_{\theta \in G} \left\{ \left| \frac{1}{N} \sum_m (\mathcal{D}_m(\theta, \lambda)) - \mathbb{E}[\mathcal{D}(\theta, \lambda)] \right| \geq \eta \right\} \right] \\ \leq (J+1) \exp \left( -\frac{2N\eta^2}{(16\sigma T|\theta - \lambda|)^2} \right). \end{aligned} \quad (\text{D.23})$$

Upper-bounding the entire thing with  $\xi$ , we obtain

$$\eta \geq \frac{16\sigma T|\theta - \lambda|}{\sqrt{2N}} \ln^{1/2} \left( \frac{J+1}{\xi} \right). \quad (\text{D.24})$$

Let  $\delta = \frac{16}{\sqrt{2N}} \ln^{1/2} \left( \frac{J+1}{\xi} \right)$ , then rearranging the terms, we see that

$$N \in \mathcal{O} \left( \frac{1}{\delta^2} \ln \left( \frac{1}{\kappa\xi} \right) \right), \quad (\text{D.25})$$

and that  $\eta = \sigma T\delta|\theta - \lambda|$ .  $\square$

### b. Main proof

We can now prove our main result. The high level proof idea is to provide upper bounds for  $\mathcal{L}(\theta)$  when  $|\theta - \lambda| \leq \kappa$  and lower bounds for  $\tilde{\mathcal{L}}(\theta)$  when  $|\theta - \lambda| \geq 2\kappa$  to ensure that minimizing  $\mathcal{L}(\theta)$  provides a close enough estimate of  $\lambda$ . To do this, we connect  $\tilde{\mathcal{L}}(\theta)$  to the ideal error function  $\mathcal{E}(\theta)$  via bounding the sampling error and truncation errors derived in the previous section. Lastly, we provide quadratic upper and lower bounds on  $\mathcal{E}(\theta)$  when applicable to provide the  $M^2N \in \tilde{\mathcal{O}}(\epsilon^{-2})$  invariance by setting  $\epsilon = 2\kappa$ .

**Theorem 3 (GLSAE).** *Fix a tuning parameter  $\beta \in [0, 1]$ , a target precision  $\epsilon > 0$  and set the range parameter  $\zeta \in \tilde{\mathcal{O}}(\epsilon^{2-2\beta})$ . Then, with high probability, there exists a quantum algorithm GLSAE that outputs an estimate  $\tilde{a}$  of  $a = \|P|\psi\rangle\|^2$ , for any  $a \in [\zeta, 1 - \zeta]$ , such that  $|\tilde{a} - a| \leq \epsilon$ . Moreover, GLSAE requires a maximum circuit depth  $M \in \tilde{\mathcal{O}}(\epsilon^{-1+\beta})$  and  $N \in \tilde{\mathcal{O}}(\epsilon^{-2\beta})$  parallel circuit samples.*

*Proof.* Recall that  $M = \lfloor \sigma T \rfloor$ . For ease of proof, we view the algorithm through the lens of  $T$  instead of  $M$ . Further recall that the values of  $\theta$  are obtained via grid search with spacing  $\kappa$ .

We first show that we can construct cases where  $\max_{|\theta - \lambda| \leq \kappa} \mathcal{L}(\theta) \leq \min_{|\theta - \lambda| \geq 2\kappa} \mathcal{L}(\theta)$ .

From [Lemma D.2](#), we can see that with probability greater than  $1 - \xi$ ,

$$\left| \left( \tilde{\mathcal{L}}(\theta) - \tilde{\mathcal{L}}(\lambda) \right) - \left( \mathbb{E}[\mathcal{L}(\theta)] - \mathbb{E}[\mathcal{L}(\lambda)] \right) \right| \leq \sigma T\delta|\theta - \lambda| \quad (\text{D.26})$$

Rearranging the terms, we find that

$$\begin{aligned} \tilde{\mathcal{L}}(\theta) &\leq \tilde{\mathcal{L}}(\lambda) + \mathbb{E}[\mathcal{L}(\theta)] - \mathbb{E}[\mathcal{L}(\lambda)] + \sigma T\delta|\theta - \lambda| \\ \tilde{\mathcal{L}}(\theta) &\geq \tilde{\mathcal{L}}(\lambda) + \mathbb{E}[\mathcal{L}(\theta)] - \mathbb{E}[\mathcal{L}(\lambda)] - \sigma T\delta|\theta - \lambda| \end{aligned} \quad (\text{D.27})$$

From [Lemma D.1](#), we obtain

$$-2\delta'^2 \leq \left( \mathbb{E}[\mathcal{L}(\theta)] - \mathbb{E}[\mathcal{L}(\lambda)] \right) - \left( \mathcal{F}(\theta) - \mathcal{F}(\lambda) \right) \leq 2\delta'^2. \quad (\text{D.28})$$

Let  $\delta' = \delta$  such that  $N \in \mathcal{O}(\frac{1}{\delta^2} \log(\frac{1}{\kappa\xi}))$  and  $\sigma \in \Omega(\log^{\frac{1}{2}}(\frac{1}{\xi}))$ . From the definition of  $\mathcal{F}$ , we note that  $\mathcal{F}(\theta) - \mathcal{F}(\lambda) = \mathcal{E}(\theta) - \mathcal{E}(\lambda) = \mathcal{E}(\theta)$ . Hence, we can write

$$\begin{aligned} \tilde{\mathcal{L}}(\theta) &\leq \tilde{\mathcal{L}}(\lambda) + \mathcal{E}(\theta) + \sigma T\delta|\theta - \lambda| + 2\delta^2 \\ \tilde{\mathcal{L}}(\theta) &\geq \tilde{\mathcal{L}}(\lambda) + \mathcal{E}(\theta) - \sigma T\delta|\theta - \lambda| - 2\delta^2 \end{aligned} \quad (\text{D.29})$$

We now discuss the following two cases:

CASE 1:  $|\theta - \lambda| \leq \kappa$ .

In this case, we provide an upper bound for  $\mathcal{E}(\theta)$  by showing smoothness bounds for both  $\mathcal{E}_1(\theta)$  and  $\mathcal{E}_2(\theta)$ . When  $T \geq 2/\pi$ , by smoothness properties in [Lemmas C.2](#) and [C.3](#),

$$\begin{aligned} \mathcal{E}_1(\theta) &= 1 - \Phi_T(2(\theta - \lambda)) \\ &\leq 1 - \Phi_T(0) - \Phi_T'(0) \times (2(\theta - \lambda)) + \frac{T^2}{2}(2(\theta - \lambda))^2 \\ &= \frac{T^2}{2}(2(\theta - \lambda))^2 \leq 2T^2\kappa^2 \end{aligned} \quad (\text{D.30})$$

Further, again by smoothness properties in [Lemmas C.2](#) and [C.3](#),

$$\begin{aligned} \mathcal{E}_2(\theta) &= \frac{\Phi_T(4\lambda)}{2} - \Phi_T(2(\theta + \lambda)) + \frac{\Phi_T(4\theta)}{2} \\ &\leq \frac{T^2}{8}(2(\theta - \lambda))^2 \leq \frac{T^2\kappa^2}{2} \end{aligned} \quad (\text{D.31})$$

Combining the results with the sampling and truncation error bounds in [Eq. \(D.29\)](#), we obtain an upper bound on  $\tilde{\mathcal{L}}(\theta)$  such that

$$\tilde{\mathcal{L}}(\theta) \leq \tilde{\mathcal{L}}(\lambda) + \frac{5}{2}T^2\kappa^2 + \sigma T\delta\kappa + 2\delta^2 \quad (\text{D.32})$$

CASE 2:  $|\theta - \lambda| \geq 2\kappa$ .

In this case, we provide a lower bound for  $\mathcal{E}(\theta)$ . By convexity from [Lemma C.1](#), when  $a \in [\frac{1}{T}, 2\pi - \frac{1}{T}]$ ,  $\Phi_T$  is convex, thus

$$\mathcal{E}_2(\theta) = \frac{\Phi_T(4\lambda)}{2} - \Phi_T(2(\theta + \lambda)) + \frac{\Phi_T(4\theta)}{2} \geq 0. \quad (\text{D.33})$$

Further, when  $T \geq 2/\pi$  and if  $2\kappa \leq \frac{1}{2T}$ , by strong convexity from [Lemma C.5](#),

$$\begin{aligned} \mathcal{E}_1(\theta) &= 1 - \Phi_T(2(\theta - \lambda)) \\ &\geq 1 - \Phi_T(0) - \Phi'_T(0) \times 2(\theta - \lambda) + \frac{T^2}{4}(2(\theta - \lambda))^2 \\ &= \frac{T^2}{4}(2(\theta - \lambda))^2 \geq 4T^2\kappa^2 \end{aligned} \quad (\text{D.34})$$

Combining the results with sampling and truncation error bounds in [Eq. \(D.29\)](#), we obtain an lower bound on  $\tilde{\mathcal{L}}(\theta)$  such that

$$\tilde{\mathcal{L}}(\theta) \geq \tilde{\mathcal{L}}(\lambda) + 4T^2\kappa^2 - 2\sigma T\delta\kappa - 2\delta^2. \quad (\text{D.35})$$

We can then see that

$$\begin{aligned} \max_{|\theta - \lambda| \leq \kappa} \tilde{\mathcal{L}}(\theta) &\leq \tilde{\mathcal{L}}(\lambda) + \frac{5}{2}T^2\kappa^2 + \sigma T\delta\kappa + 2\delta^2 \\ \min_{|\theta - \lambda| \geq 2\kappa} \tilde{\mathcal{L}}(\theta) &\geq \tilde{\mathcal{L}}(\lambda) + 4T^2\kappa^2 - 2\sigma T\delta\kappa - 2\delta^2 \end{aligned} \quad (\text{D.36})$$

Solving for

$$\frac{5}{2}T^2\kappa^2 + \sigma T\delta\kappa + 2\delta^2 \leq 4T^2\kappa^2 - 2\sigma T\delta\kappa - 2\delta^2, \quad (\text{D.37})$$

we obtain the inequality

$$\frac{3}{2}T^2\kappa^2 - 3\sigma T\delta\kappa - 4\delta^2 \geq 0, \quad (\text{D.38})$$

and

$$T \geq \frac{3\sigma\delta\kappa + \delta\kappa\sqrt{9\sigma^2 + 24}}{3\kappa^2} = \frac{\delta}{\kappa} \frac{3\sigma + \sqrt{9\sigma^2 + 24}}{3}, \quad (\text{D.39})$$

in order to fulfill  $\max_{|\theta - \lambda| \leq \kappa} \tilde{\mathcal{L}}(\theta) \leq \min_{|\theta - \lambda| \geq 2\kappa} \tilde{\mathcal{L}}(\theta)$ .

Rearranging the terms and plugging in the relevant factors, we find

$$T \in \mathcal{O} \left( \frac{1}{\sqrt{N}\kappa} \log^{\frac{1}{2}} \left( \frac{1}{\kappa\xi} \right) \log^{\frac{1}{2}} \left( \frac{N}{\log(\kappa^{-1}\xi^{-1})} \right) \right). \quad (\text{D.40})$$

The above setting of  $T$  ensures that for all  $|\theta - \lambda| \geq 2\kappa$ , the loss function is larger than that of all  $|\theta - \lambda| \leq \kappa$ . However, there still exists an annulus where  $\kappa \leq |\theta - \lambda| \leq 2\kappa$ , where the behavior is undefined. By setting  $\epsilon = 2\kappa$ , we let

$$\theta^* = \arg \min_{\theta \in G} \tilde{\mathcal{L}}(\theta) \quad (\text{D.41})$$

then per inequality above, we know that  $\theta^*$  must lie within  $\epsilon = 2\kappa$  of  $\lambda$ .

To recover the asymptotics of  $M$  and  $N$  in terms of  $\epsilon$  as in the main theorem statement, we plug in  $M = \lceil \sigma T \rceil$  and  $\epsilon = 2\kappa$  to obtain

$$M \in \mathcal{O} \left( \frac{1}{\sqrt{N}\epsilon} \log^{\frac{1}{2}} \left( \frac{1}{\xi\epsilon} \right) \log \left( \frac{N}{\log(\xi^{-1}\epsilon^{-1})} \right) \right). \quad (\text{D.42})$$

We fix a tuning parameter  $\beta \in [0, 1]$  such that  $N \in \tilde{\mathcal{O}}(\epsilon^{-2\beta})$ . We can then find that  $M \in \tilde{\mathcal{O}}(\epsilon^{-1+\beta})$ .

Lastly, we note that as the  $\epsilon$  is the bound for the phase difference  $|\theta - \lambda|$ , we still need to relate it back to the amplitude  $\tilde{a} = \sin^2(\theta) = \frac{1 - \cos(2\theta)}{2}$ . From Lipschitz bounds, we see that

$$|\cos(x) - \cos(y)| \leq |x - y|. \quad (\text{D.43})$$

Hence, we can obtain

$$|\tilde{a} - a| \leq |\theta - \lambda| \leq \epsilon. \quad (\text{D.44})$$

From the valid range of  $\theta$  and  $\lambda$  from maintaining  $\mathcal{E}_2(\theta) \geq 0$ , we require  $\theta, \lambda \in [\frac{1}{4T}, \frac{\pi}{2} - \frac{1}{4T}]$  so the valid range for estimating  $a$  is then  $[\sin^2(\frac{1}{4T}), \cos^2(\frac{1}{4T})]$ . Setting  $\zeta = \sin^2(\frac{1}{4T})$ , we find that

$$\sin^2 \left( \frac{1}{4T} \right) \leq \frac{1}{16T^2} \in \tilde{\mathcal{O}}(\epsilon^{2-2\beta}). \quad (\text{D.45})$$

□

We further provide specific results regarding the runtime at the Heisenberg limit range where  $M \in \mathcal{O}(\frac{1}{\epsilon})$ .

**Corollary 3.1.** *Fixing  $\beta = 0$ , with high probability, GLSAE outputs an estimate  $\tilde{a}$  of  $a = \|P|\psi\rangle\|^2$ , for any  $a \in [0, 1]$ , such that  $|\tilde{a} - a| \leq \epsilon$ . GLSAE requires a maximum circuit depth  $M \in \mathcal{O}(\epsilon^{-1})$  and  $N \in \mathcal{O}(\log(\epsilon^{-1}))$  parallel circuit samples.*

*Proof.* Let  $N \in \mathcal{O}(\log(\xi^{-1}\epsilon^{-1}))$ . [Eq. \(D.42\)](#) produces  $M \in \mathcal{O}(\epsilon^{-1})$ . In this regime, we note that  $\zeta \in \tilde{\mathcal{O}}(\epsilon^2)$ , and thus, we have  $\zeta \geq \epsilon$ . As a result, even when  $a \in [0, \zeta]$ , the estimate  $\tilde{a}$  found would be either 0 or  $\epsilon$ , both of which are valid outputs. The same follows for  $a \in [1 - \zeta, 1]$ . Thus, when  $\beta = 0$ , the range of estimation for  $a$  is over the entire  $[0, 1]$ . □

## Appendix E: Further details on GDMAE

In GLSAE, we note that there exists a region where  $\theta$  is close to 0 or  $\pi/2$  (or equivalently,  $a$  is close to 0 or 1) where we cannot discern the minimum of the loss function easily, and note that this stems from overlapping Gaussians centered around either  $\lambda$  and  $-\lambda$  or  $\lambda$  and  $\pi - \lambda$ . This is a result of only having access to cosine signals. Thus, to resolve this issue of the indiscernibility of twin Gaussian peaks, we require access to the sine signals as well. GDMAE provides this via an extra measurement in the Pauli X basis.

### 1. Algorithm and discussions for GDMAE

As mentioned in the main text, we discuss a particular type of amplitude estimation problem where the input

state takes the form of

$$|\psi\rangle = \sin(\lambda) |\psi_g\rangle |1\rangle + \cos(\lambda) |\psi_b\rangle |0\rangle, \quad (\text{E.1})$$

where there exists a flag qubit such that one can easily discern between good and bad states via readout of the flag qubit.

Making use of this structure, we can obtain, for odd-degree outputs, the following signal via Pauli-X measurements.

$$\begin{aligned} & \langle \psi | Q^{-t} (\mathbb{I} \otimes X) Q^t | \psi \rangle \\ &= (\sin((2t+1)\lambda) \langle \psi_g | \langle 1 | + \cos((2m+1)\lambda) \langle \psi_b | \langle 0 |) \\ & \quad (\mathbb{I} \otimes X) \\ & \quad (\sin((2t+1)\lambda) |\psi_g\rangle |1\rangle + \cos((2m+1)\lambda) |\psi_b\rangle |0\rangle) \\ &= 2 \sin((2t+1)\lambda) \cos((2t+1)\lambda) \\ &= \sin((4t+2)\lambda) \end{aligned} \quad (\text{E.2})$$

This can only be done for cases where we can create a transition operator, in the case above, a Pauli-X that transitions between the subspace occupied by the good state and the subspace occupied by the bad state. For the case of even degrees, we do not have an efficient transition operator for  $|\psi\rangle$  and  $|\perp\rangle$  without adding an extra qubit. However, this alone suffices to provide enough information to cancel out the cross terms.

We note that if we *do* allow an extra qubit here on top of the flag qubit at the very end, we can use a multi-controlled Toffoli gate to flip the additional qubit only when the main register (inclusive of the flag qubit) is in the zero state after applying the Loschmidt echo circuit, and then do a Pauli-X measurement on the additional qubit. This is still relatively cheap, as we do not require controlled unitaries, but the protocol is no longer ancilla-free.

We now show the Gaussian Dual Measurement Amplitude Estimation (GDMAE) algorithm. We discard the use of Loschmidt echo circuits used GLSAE entirely due to the inability to provide a sine signal without adding an extra qubit, as mentioned above. In this scheme, we focus only on the “standard” amplitude amplification circuits. We hence define a new probability distribution to sample from

$$\tilde{q}_T(m) = \begin{cases} \frac{2}{\sqrt{2\pi T \tilde{Z}}} \exp\left(-\frac{m^2}{2T^2}\right) & m \text{ is odd, } |m| \leq \sigma T \\ 0 & m \text{ is even, } m \neq 0 \\ 0 & |m| > \sigma T \\ 1 - \sum_{\tau \neq 0} \tilde{q}_T(\tau) & m = 0 \end{cases} \quad (\text{E.3})$$

where  $\tilde{Z}$  is the same as that of GLSAE. A minor, but important detail, is that if the normalization factor is taken to be  $\tilde{W} = \sum_{m=-M, m \text{ is odd}}^M \frac{1}{\sqrt{2\pi T}} e^{-\frac{m^2}{2T^2}}$  instead of  $\tilde{Z}/2$ , the algorithm would not work in low depths due to amplified numerical and truncation errors under normalization of  $\tilde{W}$ .

We then sample from both the standard amplified amplification circuit with the Pauli Z measurement, denoting

---

**Algorithm 2:** Gaussian Dual Measurement Amplitude Estimation (GDMAE)

---

**Input:** State  $|\psi\rangle$ , Projector  $P$ , Walk operator  $Q$ , Gaussian width  $T$ , Maximum circuit depth  $M$ , Number of parallel queries  $N$ , Precision  $\epsilon$

**Output:** Estimate of  $a = \|P|\psi\rangle\|^2$

1 Sample  $N$  iterations  $m$  from truncated discrete Gaussian

$$\tilde{q}_T(m) = \begin{cases} \frac{2}{\sqrt{2\pi T \tilde{Z}}} \exp\left(-\frac{m^2}{2T^2}\right) & m \text{ is odd, } |m| \leq M \\ 0 & m \text{ is even, } m \neq 0 \\ 0 & |m| > M \\ 1 - \sum_{\tau \neq 0} \tilde{q}_T(\tau) & m = 0 \end{cases}$$

2 **for** each sampled  $m$  out of  $N$  samples where

$|m| = 2t + 1, t \in \mathbb{Z}_{\geq 0}$  **do**  
    3 Measure Pauli observable  $Z$  on the flag qubit with state  $Q^t |\psi\rangle$  and obtain  $Z_m \in \{\pm 1\}$   
    4 Measure Pauli observable  $X$  on the flag qubit with state  $Q^t |\psi\rangle$  and obtain  $X_{|m|} \in \{\pm 1\}$   
    5 **if**  $m < 0$  **then**  
    6      $X_m = -X_{|m|}$

7 Obtain estimate  $\tilde{\lambda}$  of  $\lambda$  from

$$\begin{aligned} \tilde{\lambda} &= \arg \max_{\theta \in [0, \frac{\pi}{2}]} \tilde{\mathcal{M}}(\theta) \\ &= \arg \max_{\theta \in [0, \frac{\pi}{2}]} \frac{1}{N} \sum_{m \sim \tilde{q}_T} (Z_m \cos(2\theta m) + X_m \sin(2\theta m))^2 \end{aligned}$$

via a two-level grid search for  $\chi^*$  across

$$\theta \in \left\{ \frac{\pi \chi}{2M} : \chi \in [M] \right\}$$

followed by a more fine-grained search for  $\eta^*$  across

$$\theta \in \left\{ \frac{\pi \chi^*}{2M} + \frac{\eta \epsilon}{3} : \eta \in \left[ -\frac{12\pi}{M\epsilon}, \frac{12\pi}{M\epsilon} \right] \right\}$$

8 **return**  $\tilde{a} = \sin^2(\tilde{\lambda})$  up to additive precision  $\epsilon$

---

the output as  $Z_m$ , and the modified amplified amplification circuit with the Pauli X measurement, denoting the output as  $X_m$ . Note that if we sample a negative  $m$ , for the cosine signal, we proceed similarly as GLSAE by ignoring the sign and set  $Z_{-m} = Z_m$ , but for the sine signal, we need to flip the sign of the estimate such that  $X_{-m} = -X_m$  due to sine being an odd function. We maximize a magnitude function

$$\tilde{\mathcal{M}}(\theta) = \frac{1}{N} \sum_{m \sim \tilde{q}_T} Z_m \cos(2\theta m) + X_m \sin(2\theta m) \quad (\text{E.4})$$

again by the two-level grid search in GLSAE with grid spacing  $\kappa = \frac{\epsilon}{3}$ . Considering the expected value of the

magnitude function, we find that we have

$$\begin{aligned}\mathbb{E}[\tilde{\mathcal{M}}(\theta)] &= \mathbb{E}[Z_m \cos(2\theta m) + X_m \sin(2\theta m)] \\ &= \mathbb{E}[\cos(2\lambda m) \cos(2\theta m) + \sin(2\lambda m) \sin(2\theta m)] \\ &= \mathbb{E}[\cos(2(\theta - \lambda)m)],\end{aligned}\quad (\text{E.5})$$

resolving the problem of having an alternative peak. We summarize the algorithm in [Algorithm 2](#).

For completeness, we detail the distinction between GDMAE and the Hadamard test. While both involve Pauli measurements on an ancilla, their operational roles differ. The Hadamard test extracts phase information via controlled unitary evolution and interferometric readout. In contrast, GDMAE does not rely on controlled time-evolution operators; the flag qubit is embedded within the state-preparation circuit and encodes amplitude information rather than serving as a phase probe.

While combining the Hadamard test with amplitude amplification also fits in the GDMAE framework, our framework encompasses a larger family of problems beyond the Hadamard test. A prominent example is quantum Monte Carlo mean estimation [36]. Consider the standard state-preparation procedure where we have access to a unitary that prepares  $\mathbf{y}$  in its binary representation in superposition, also known as “having the source code” to  $\mathbf{y}$  [37] as follows:

$$\begin{aligned}& \frac{1}{\sqrt{N}} \sum_j |j\rangle |0\rangle |0\rangle \\ & \xrightarrow{\text{compute}} \frac{1}{\sqrt{N}} \sum_j |j\rangle |y_j\rangle |0\rangle \\ & \xrightarrow{\text{controlled rotations}} \frac{1}{\sqrt{N}} \sum_j |j\rangle |y_j\rangle (\sqrt{y_j} |1\rangle + \sqrt{1-y_j} |0\rangle) \\ & \xrightarrow{\text{uncompute}} \frac{1}{\sqrt{N}} \sum_j |j\rangle |0\rangle (\sqrt{y_j} |1\rangle + \sqrt{1-y_j} |0\rangle),\end{aligned}\quad (\text{E.6})$$

where we encode  $\mathbf{y}$  into amplitudes through controlled rotations for mean estimation. This construction does not reduce to a Hadamard-test architecture. Within this setting, GDMAE can be applied to estimate  $\|\mathbf{y}\|_1$  by measuring both a Pauli Z and X on the flag qubit.

## 2. Proofs for GDMAE

Due to the fact that we only have access to “standard” amplitude amplification circuits, we first discuss the effects of discrete-time cosine transform would have when the filter function is  $\tilde{q}_T$  instead of  $\tilde{p}_T$ . Instead of a periodic Gaussian, the transformed function is a periodic Gaussian with peaks of alternating signs as shown in [Fig. 7](#). We discuss the construction and the corresponding smoothness and strongly concave properties in the following, before moving on to the main proof of GDMAE.

### a. Construction and properties of the alternating-sign periodic Gaussian

For this section, let us first take a closer look at the alternative sampling distribution that discards even-degree signals, as well as the resulting function from a discrete-time cosine transform. We first consider the unnormalized discrete Gaussian

$$r_T(m) = \frac{1}{\sqrt{2\pi T}} \exp\left(-\frac{m^2}{2T^2}\right) = \mathcal{Z} \cdot p_T(m) \quad (\text{E.7})$$

which, after a discrete-time cosine transform, becomes the periodic Gaussian

$$\sum_{m=-\infty}^{\infty} r_T(m) \cos(km) = \sum_{j \in \mathcal{Z}} \exp\left(-\frac{(k + 2j\pi)^2 T^2}{2}\right). \quad (\text{E.8})$$

Now, instead of taking the infinite sum over  $\cos(km)$ , we cancel out the even terms by taking

$$\sum_{m=-\infty}^{\infty} \frac{r_T(m)}{2} (\cos(km) - (-1)^m \cos(km)). \quad (\text{E.9})$$

We note that when  $m \in \mathcal{Z}$ , the latter term can be written as

$$(-1)^m \cos(km) = \cos((k + \pi)m). \quad (\text{E.10})$$

Thus, we have

$$\begin{aligned}& \sum_{m=-\infty}^{\infty} \frac{r_T(m)}{2} (\cos(km) - \cos((k + \pi)m)) \\ &= \frac{1}{2} \sum_{j \in \mathcal{Z}} \exp\left(-\frac{(k + 2j\pi)^2 T^2}{2}\right) \\ & \quad - \frac{1}{2} \sum_{j \in \mathcal{Z}} \exp\left(-\frac{(k + (2j + 1)\pi)^2 T^2}{2}\right).\end{aligned}\quad (\text{E.11})$$

Now, consider the normalized discrete Gaussian without even terms as follows:

$$q_T(m) = \begin{cases} \frac{2}{\sqrt{2\pi T \mathcal{Z}}} \exp\left(-\frac{m^2}{2T^2}\right) & m \text{ is odd} \\ 0 & m \text{ is even, but not } 0 \\ 1 - \sum_{\tau \in \mathcal{Z} \setminus \{0\}} q_T(\tau) & m = 0 \end{cases} \quad (\text{E.12})$$

where  $\mathcal{Z} = \sum_{m=-\infty}^{\infty} \frac{1}{\sqrt{2\pi T}} \exp(-\frac{m^2}{2T^2})$ . We can then see that the discrete-time cosine transform of  $q_T(m)$ ,

$$\begin{aligned}\Psi_T(k) &= \sum_{m=-\infty}^{\infty} q_T(m) \cos(km) \\ &= \frac{1}{\mathcal{Z}} \sum_{m=-\infty}^{\infty} r_T(m) (\cos(km) - \cos((k + \pi)m)) + q_T(0) \\ &= \sum_{m=-\infty}^{\infty} p_T(m) (\cos(km) - \cos((k + \pi)m)) + q_T(0)\end{aligned}$$

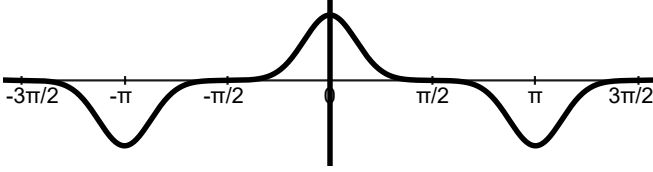


FIG. 7. Alternating sign periodic Gaussian from discrete-time cosine transform of  $q_T$ .

$$= \Phi_T(k) - \Phi_T(k + \pi) + q_T(0) \quad (\text{E.13})$$

where we can see that

$$\Psi_T(k) = \sum_{m=-\infty}^{\infty} q_T(m) \cos(km) \leq \sum_{m=-\infty}^{\infty} q_T(m) = 1. \quad (\text{E.14})$$

This takes the form of a periodic Gaussian with alternating signed peaks every  $\pi$ , as shown in Fig. 7.

For sanity checking, we show that  $\mathcal{Z}/2$  is indeed a suitable normalization factor when we sample only odd points:

$$\begin{aligned} \mathcal{W} &= \sum_{m=-\infty, m \text{ is odd}}^{\infty} \frac{1}{\sqrt{2\pi T}} e^{-\frac{m^2}{2T^2}} \\ &= \sum_{m=-\infty}^{\infty} \frac{1}{\sqrt{2\pi T}} e^{-\frac{m^2}{2T^2}} - \sum_{t=-\infty}^{\infty} \frac{1}{\sqrt{2\pi T}} e^{-\frac{(2t)^2}{2T^2}} \\ &= \sum_{m=-\infty}^{\infty} \frac{1}{\sqrt{2\pi T}} e^{-\frac{m^2}{2T^2}} - \sum_{t=-\infty}^{\infty} \frac{(1/2)}{\sqrt{2\pi(T/2)}} e^{-\frac{t^2}{2(T/2)^2}} \\ &= \mathcal{Z}_T - \frac{1}{2} \mathcal{Z}_{\frac{T}{2}} \leq \frac{1}{2} \mathcal{Z}_T \end{aligned} \quad (\text{E.15})$$

With this, we can also further note that  $q_T(0) = 1 - \frac{2\mathcal{W}}{\mathcal{Z}}$ . For the actual implementation, we again truncate at  $\sigma\tilde{T}$  to limit the maximum circuit depth and replace  $\mathcal{Z}$  with  $\tilde{\mathcal{Z}}$  to form the actual sampling distribution  $\tilde{q}_T$  in Eq. (E.3).

Using  $\tilde{\mathcal{Z}}$  as the normalization factor instead of the sum over odd  $m$ -s is of vital importance for the low-depth algorithm in practice. For low-depth settings where the sampling Gaussian has a low standard deviation  $T$ , a large portion of the samples concentrates on  $m = 0$ . Hence, if we only filter out the even  $m$  samples and normalize over odd  $m$ -s, this produces a high numerical instability where the errors of the probability distribution from truncation, or even limited floating point representations, can be amplified many-fold, given that a large portion of the original samples are thrown out. These amplified errors would then be introduced into the final amplitude estimate.

We now show the smoothness and strongly concave properties of  $\Psi_T$ .

**Lemma E.1.** *Let  $T \geq 2/\pi$ , then  $\Psi_T$  is  $2T^2$ -smooth.*

*Proof.* As we can write

$$\Psi_T(x) = \Phi_T(x) - \Phi_T(x + \pi) + 1 - \frac{2\mathcal{W}}{\mathcal{Z}}, \quad (\text{E.16})$$

taking the second derivative, we obtain

$$\Psi_T''(x) = \Phi_T''(x) - \Phi_T''(x + \pi). \quad (\text{E.17})$$

By the triangle inequality, we then get

$$|\Psi_T''(x)| = |\Phi_T''(x)| + |\Phi_T''(x + \pi)|. \quad (\text{E.18})$$

By Lemma C.3, we then upper bound the right-hand side by  $2T^2$ , completing the proof.  $\square$

**Lemma E.2.** *Let  $T \geq 2/\pi$ , then  $\Psi_T$  is  $\frac{T^2}{2}$ -strongly concave on the interval  $[-\frac{1}{2T}, \frac{1}{2T}]$ .*

*Proof.* Again starting from

$$\Psi_T(x) = \Phi_T(x) - \Phi_T(x + \pi) + 1 - \frac{2\mathcal{W}}{\mathcal{Z}}, \quad (\text{E.19})$$

we know from Lemma C.5 that  $\Phi_T''(x)$  is  $\frac{T^2}{2}$ -strongly concave on the interval  $[-\frac{1}{2T}, \frac{1}{2T}]$ . Then by Lemma C.1, we can note that  $-\Phi_T''(x)$  is concave on  $[\frac{1}{T}, 2\pi - \frac{1}{T}]$ , hence  $-\Phi_T''(x + \pi)$  is concave on  $[\frac{1}{T} - \pi, \pi - \frac{1}{T}]$ . Combining the two, we see that  $\Psi_T(x)$  is  $\frac{T^2}{2}$ -strongly concave on the interval  $[-\frac{1}{2T}, \frac{1}{2T}]$ .  $\square$

b. *Truncation and sampling errors of the magnitude function*

We define the magnitude function

$$\mathcal{M}_m(\theta) = Z_m \cos(2\theta m) + X_m \sin(2\theta m), \quad (\text{E.20})$$

where the sample magnitude can be defined as

$$\tilde{\mathcal{M}}(\theta) = \frac{1}{N} \sum_m Z_m \cos(2\theta m) + X_m \sin(2\theta m). \quad (\text{E.21})$$

Again, in an abuse of notation, we drop the subscript for  $\mathcal{M}_m$  when  $m$  is arbitrary. We find that we have

$$\begin{aligned} \mathbb{E}[\mathcal{M}(\theta)] &= \mathbb{E}[\cos(2\lambda m) \cos(2\theta m) + \sin(2\lambda m) \sin(2\theta m)] \\ &= \mathbb{E}[\cos(2(\theta - \lambda)m)]. \end{aligned} \quad (\text{E.22})$$

The following theorem shows that the expected value of  $\mathcal{M}(\theta)$  is close to the alternating signed periodic Gaussian by a truncation error. This implies that the quadratic upper and lower bounds can be directly applied with no regions of failure.

**Lemma E.3.** *Given  $\delta > 0$ , if  $\sigma \in \Omega(\log^{\frac{1}{2}}(\frac{1}{\delta}))$  and  $\rho \geq \sigma$ , we have*

$$|\mathbb{E}[\mathcal{M}(\theta)] - \Psi_T(2(\theta - \lambda))| \leq \delta^2 \quad (\text{E.23})$$

*Proof.* Similar to Lemma D.1, we wish to find the truncation error. Noting that

$$\begin{aligned} |\mathbb{E}[\mathcal{M}(\theta)] - \Psi(2(\theta - \lambda))| \\ = |\mathbb{E}[\cos(2(\theta - \lambda)m)] - \Psi(2(\theta - \lambda))|, \end{aligned} \quad (\text{E.24})$$

we let  $\gamma = 2(\theta - \lambda)$  and compute the following:

$$\begin{aligned}
& |\mathbb{E}[\cos(\gamma m)] - \Psi_T(\gamma)| \\
&= \left| \sum_{|m| \leq \sigma T} \tilde{q}_T(m) \cos(\gamma m) - \sum_{m=-\infty}^{\infty} q_T(m) \cos(\gamma m) \right| \\
&\leq \left| \frac{\mathcal{Z} - \tilde{\mathcal{Z}}}{\tilde{\mathcal{Z}}} \sum_{m=-\infty}^{\infty} q_T(m) \cos(\gamma m) + \frac{\tilde{\mathcal{Z}} - \mathcal{Z}}{\tilde{\mathcal{Z}}} \right. \\
&\quad \left. + \sum_{|m| > \sigma T} \frac{\mathcal{Z}}{\tilde{\mathcal{Z}}} q_T(m) (1 - \cos(\gamma m)) \right| \\
&\leq \left| \frac{\mathcal{Z} - \tilde{\mathcal{Z}}}{\tilde{\mathcal{Z}}} (\Psi_T(\gamma) - 1) \right| + \sum_{|m| > \sigma T} \left| \frac{\mathcal{Z}}{\tilde{\mathcal{Z}}} q_T(m) (1 - \cos(\gamma m)) \right| \\
&\leq 2 \left| \frac{\mathcal{Z} - \tilde{\mathcal{Z}}}{\tilde{\mathcal{Z}}} \right| + 2 \sum_{|m| > \sigma T} \frac{\mathcal{Z}}{\tilde{\mathcal{Z}}} q_T(m). \tag{E.25}
\end{aligned}$$

We then bound the second term such that

$$\begin{aligned}
\sum_{|m| > \sigma T} \frac{\mathcal{Z}}{\tilde{\mathcal{Z}}} q_T(m) &= \sum_{|m| > \sigma T, m \text{ is odd}} \frac{2}{\sqrt{2\pi T} \tilde{\mathcal{Z}}} e^{-\frac{m^2}{2T^2}} \\
&\leq \sum_{|m| > \sigma T} \frac{2}{\sqrt{2\pi T}} e^{-\frac{m^2}{2T^2}} \\
&\leq 4 \int_{m=\sigma T}^{\infty} \frac{1}{\sqrt{2\pi T}} e^{-\frac{m^2}{2T^2}} dt \\
&= \int_{s=\sigma}^{\infty} 2\sqrt{\frac{2}{\pi}} e^{-\frac{s^2}{2}} ds \leq 2e^{-\sigma^2} \leq \frac{\delta^2}{3} \tag{E.26}
\end{aligned}$$

Similar to [Lemma D.1](#), we bound the first term as:

$$\left| \frac{\mathcal{Z} - \tilde{\mathcal{Z}}}{\tilde{\mathcal{Z}}} \right| \leq e^{-\sigma^2} \leq \frac{\delta^2}{6}. \tag{E.27}$$

Thus, we can obtain

$$|\mathbb{E}[\cos(2(\theta - \lambda)m)] - \Psi_T(2(\theta - \lambda))| \leq \delta^2, \tag{E.28}$$

□

We again obtain bounds regarding the number of samples  $N$  via the Hoeffding bound of the difference of losses. Let

$$\mathcal{R}_m(\theta, \lambda) = \mathcal{M}_m(\theta) - \mathcal{M}_m(\lambda). \tag{E.29}$$

We then obtain the following lemma.

**Lemma E.4.** *Let  $0 \leq \xi \leq 1$ ,  $\delta \geq 0$ ,  $\lambda \in [0, \frac{\pi}{2}]$  and  $\kappa > 0$ . We define a grid  $G$  in range  $[0, \frac{\pi}{2}]$  with spacing  $\kappa$  and let  $J = \lfloor \frac{\pi}{2\kappa} \rfloor$  such that  $G = \{\frac{k}{\kappa} : k \in [J] \cup \{0\}\}$ . For all possible values of  $\theta \in G$ , if  $N \in \mathcal{O}(\frac{1}{\delta^2} \log(\frac{1}{\kappa\xi}))$ , then*

$$\Pr \left[ \left| \frac{1}{N} \sum_m (\mathcal{R}_m(\theta, \lambda)) - \mathbb{E}[\mathcal{R}(\theta, \lambda)] \right| \leq \sigma T \delta |\theta - \lambda| \right] \geq 1 - \xi.$$

*Proof.* Expanding the difference of magnitudes, we obtain

$$\begin{aligned}
\mathcal{R}_m(\theta, \lambda) &= \mathcal{M}_m(\theta) - \mathcal{M}_m(\lambda) \\
&= Z_m(\cos(2\theta t) - \cos(2\lambda t)) \\
&\quad + X_m(\sin(2\theta t) - \sin(2\lambda t)) \tag{E.30}
\end{aligned}$$

By the Lipschitz property, we obtain the following:

$$\begin{aligned}
|\mathcal{R}_m(\theta, \lambda)| &\leq |\cos(2\theta m) - \cos(2\lambda m)| \\
&\quad + |\sin(2\theta m) - \sin(2\lambda m)| \\
&\leq 4\sigma T |\theta - \lambda| \tag{E.31}
\end{aligned}$$

where the last inequality is obtained by noting that for all  $m$ ,  $m \leq \sigma T$ . Applying the Hoeffding and union bound similar to [Lemma D.2](#), and setting  $\delta = \frac{8}{\sqrt{2N}} \ln^{1/2} \left( \frac{J+1}{\xi} \right)$  we obtain the lemma. □

### c. Main proof

We can now prove our main result. The proof idea is largely the same as [Theorem 3](#) apart from the difference in the optimization function.

**Theorem 4** (GDMAE). *Given a flag qubit as in [Eq. \(4\)](#), we can construct a quantum algorithm, GDMAE, that outputs  $\tilde{a}$  for all  $a \in [0, 1]$  such that  $|\tilde{a} - a| \leq \epsilon$  with the same asymptotic costs as [Theorem 3](#) of a maximum circuit depth  $M \in \tilde{\mathcal{O}}(\epsilon^{-1+\beta})$  and  $N \in \tilde{\mathcal{O}}(\epsilon^{-2\beta})$  parallel circuit samples. Here, the parameter  $\beta \in [0, 1]$  can be chosen arbitrarily to interpolate between Heisenberg and standard shot-noise scalings.*

*Proof.* We show that when  $|\theta - \lambda| \leq \kappa$  and  $\min_{|\theta - \lambda| \leq \kappa} \mathcal{M}(\theta) \geq \max_{|\theta - \lambda| \geq 3\kappa} \mathcal{M}(\theta)$  if  $T^2 N \in \tilde{\mathcal{O}}(\frac{1}{\epsilon^2})$ .

Let  $N \in \mathcal{O}(\frac{1}{\delta^2} \log(\frac{1}{\kappa\xi}))$  and  $\sigma \in \Omega(\log^{\frac{1}{2}}(\frac{1}{\delta}))$ . From truncation and sampling error bounds in [Lemmas E.3](#) and [E.4](#), we obtain with high probability that

$$\begin{aligned}
& |(\mathbb{E}[\mathcal{M}(\theta)] - \mathbb{E}[\mathcal{M}(\lambda)]) - (\Psi_T(2(\theta - \lambda)) - \Psi_T(0))| \\
&\leq \sigma T \delta |\theta - \lambda| + 2\delta^2. \tag{E.32}
\end{aligned}$$

We now discuss the following cases:

CASE 1:  $|\theta - \lambda| \leq \kappa$ .

When  $T \geq 2/\pi$ , by smoothness properties in [Lemmas C.2](#) and [E.1](#),

$$\begin{aligned}
-\Psi_T(2(\theta - \lambda)) &\leq -\Psi_T(0) + T^2(2(\theta - \lambda))^2 \\
&\leq -\Psi_T(0) + 4T^2\kappa^2 \tag{E.33}
\end{aligned}$$

Combining the above Hoeffding and truncation error bounds, we obtain a lower bound on  $\tilde{\mathcal{L}}(\theta)$  such that

$$\tilde{\mathcal{M}}(\theta) \geq \tilde{\mathcal{M}}(\lambda) - 4T^2\kappa^2 - \sigma T \delta \kappa - 2\delta^2 \tag{E.34}$$

CASE 2:  $|\theta - \lambda| \geq 3\kappa$ .

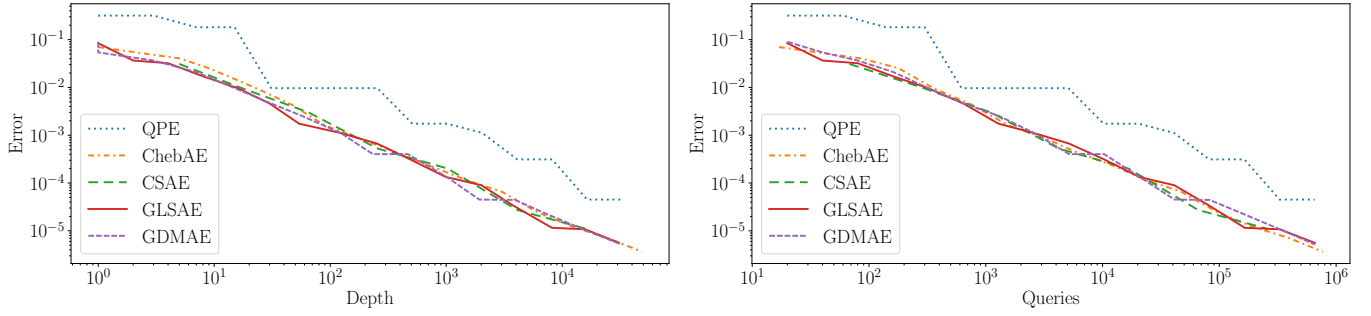


FIG. 8. Comparison of the depth and query complexity of Heisenberg-limited amplitude estimation algorithms. We benchmark both of our algorithms, GLSAE and GDMAE, against the “textbook” QPE-based algorithm [1], ChebAE from quantum signal processing [8], and CSAE from ESPRIT [10]. We note that our methods perform similarly to the prior state-of-the-art, such as ChebAE and CSAE.

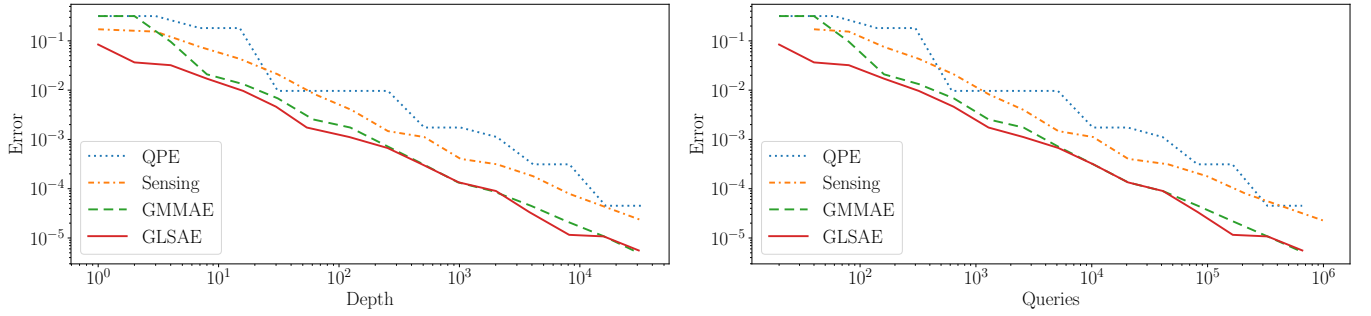


FIG. 9. Comparison of the depth and query complexity of variant algorithms inspired by other statistical phase estimation algorithms. We benchmark an additional two algorithms, one that uses compressed sensing for the classical post-processing step, and a variant of our algorithms, GMMAE, where we also only have cosine signals like GLSAE, but maximizes the magnitude function like GDMAE. We show that our highlighted methods in the main text perform better than these variant methods.

When  $T \geq 2/\pi$  and if  $3\kappa \leq \frac{1}{2T}$ , by strongly concave properties in [Lemmas C.4](#) and [E.2](#),

$$\begin{aligned} -\Psi_T(2(\theta - \lambda)) &\geq -\Psi_T(0) + \frac{T^2}{4}(2(\theta - \lambda))^2 \\ &\geq -\Psi_T(0) + 9T^2\kappa^2 \end{aligned} \quad (\text{E.35})$$

Combining the above Hoeffding and truncation error bounds, we obtain an upper bound on  $\tilde{\mathcal{L}}(\theta)$  such that

$$\tilde{\mathcal{M}}(\theta) \leq \tilde{\mathcal{M}}(\lambda) - 9T^2\kappa^2 + 2\sigma T\delta\kappa + 2\delta^2. \quad (\text{E.36})$$

To find  $\min_{|\theta - \lambda| \leq \kappa} \tilde{\mathcal{M}}(\theta) \geq \max_{|\theta - \lambda| \geq 3\kappa} \tilde{\mathcal{M}}(\theta)$ , we solve for

$$\tilde{\mathcal{M}}(\lambda) - 4T^2\kappa^2 - \sigma T\delta\kappa - 2\delta^2 \geq \tilde{\mathcal{M}}(\lambda) - 9T^2\kappa^2 + 3\sigma T\delta\kappa + 2\delta^2, \quad (\text{E.37})$$

and obtain the inequality

$$5T^2\kappa^2 - 4\sigma T\delta\kappa - 4\delta^2 \geq 0, \quad (\text{E.38})$$

which, when solved, provides

$$T \in \mathcal{O}\left(\frac{1}{\sqrt{N}\kappa} \log^{\frac{1}{2}}\left(\frac{1}{\kappa\xi}\right) \log^{\frac{1}{2}}\left(\frac{N}{\log(\kappa^{-1}\xi^{-1})}\right)\right). \quad (\text{E.39})$$

where, by applying the same arguments for the annulus in [Theorem 3](#) and by setting  $\epsilon = 3\kappa$ , we can then similarly write  $M = \lfloor \sigma T \rfloor \in \tilde{\mathcal{O}}(\epsilon^{-1+\beta})$  and  $N \in \tilde{\mathcal{O}}(\epsilon^{-2\beta})$  to satisfy the above.

With similar Lipschitz bounds as [Theorem 3](#) for the phase to amplitude, we obtain

$$|\tilde{a} - a| \leq |\theta - \lambda| \leq \epsilon. \quad (\text{E.40})$$

□

## Appendix F: Implementation details for numerics

We provide more in-depth details for our numerical results in the main text, including full depth and query complexity results, as well as alternate and extended implementations of ideas from statistical phase estimation not featured in the main text.

### 1. Heisenberg-limited amplitude estimation

In [Fig. 8](#), we show that our algorithms perform similarly to the prior state-of-the-art, such as ChebAE and

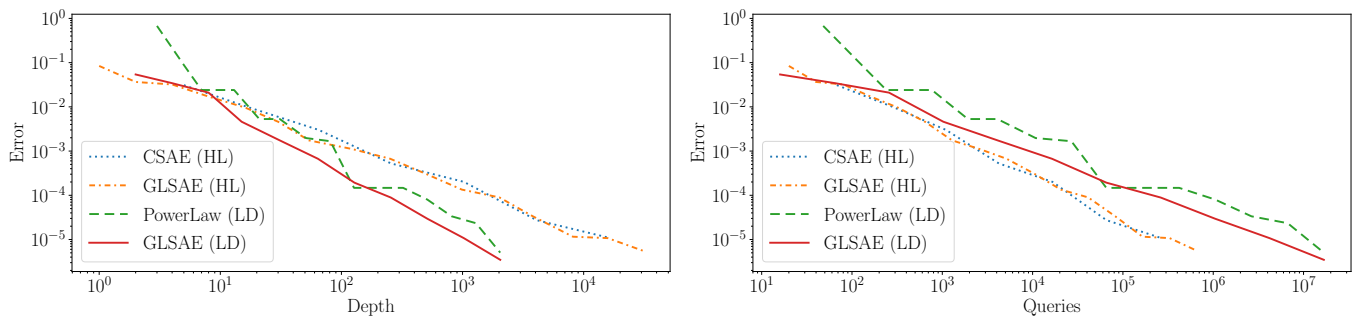


FIG. 10. Comparison of the depth and query complexity of Heisenberg-limited amplitude estimation algorithms and low-depth amplitude estimation. We set the circuit depth and circuit sample complexity of the low-depth circuits equivalent to uniform time sampling where  $\mathcal{D} \in \mathcal{O}(\epsilon^{-2/3})$  and  $\mathcal{N} \in \mathcal{O}(\epsilon^{-4/3})$ . Note that the trade off for low-depth algorithms comes at the cost of higher total query complexity.

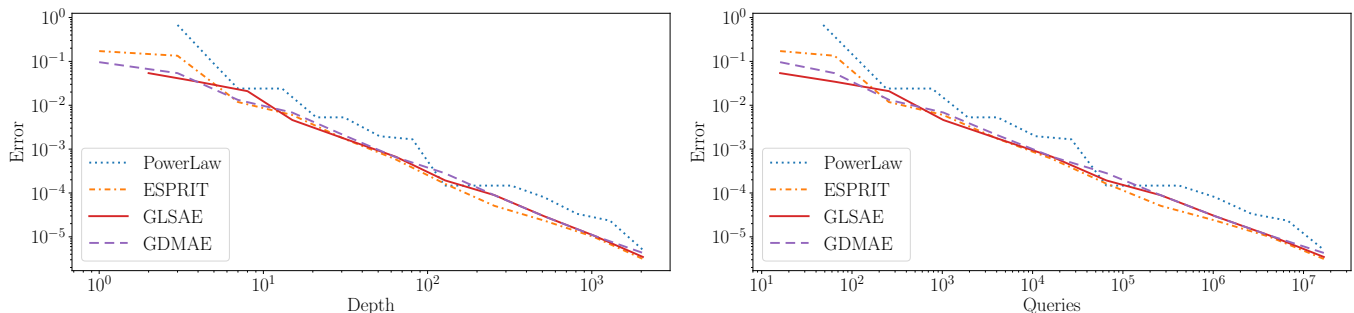


FIG. 11. Comparison of the depth and query complexity of low-depth amplitude estimation. We again set the circuit depth and circuit sample complexity to be equivalent to uniform time sampling, where we can benchmark against ESPRIT. We see that our algorithms outperform prior art such as Power law AE [12], and match ESPRIT, which has been shown to be classically efficient for signal processing under noise.

CSAE, in both depth and query complexities. Apart from our algorithms and state-of-the-art amplitude estimation algorithms, we also adapt compressed sensing [84, 85] for post-processing. Further, we also present a variant algorithm, Gaussian Maximum Magnitude Amplification Estimation, to shed light on why we use two different optimization functions for our algorithms. Relevant numerical results are shown in Fig. 9. We detail the implementation of our methods as follows:

**Compressed sensing.**— We adapt the use of compressed sensing in phase estimation from Yi *et al.* [82] to perform amplitude estimation. As our signals are a single cosine, we employ the use of a discrete Fourier transform matrix, but just the discrete cosine transform matrix. In addition, we employ the use of LASSO [97] for minimization as opposed to convex optimization with  $\ell_1$  inequality constraints, as given the high noise in the samples, the inequality constraints require a hyperparameter to control the tolerance of noise, and it might be simpler to penalize the  $\ell_1$  norm as part of the loss minimization rather than a strict constraint. From Fig. 9, we see that while compressed sensing has asymptotically similar performances (judging from the slope), it requires a higher number of both queries and depth compared to ChebAE, CSAE, and

our algorithm.

**GMMAE.**— For this algorithm, instead of taking the minimum of the loss function in GLSAE, we maximize the magnitude function in GDMAE without the addition of the sine signals, that is, we maximize

$$\tilde{\mathcal{M}}'(\theta) = \frac{1}{N} \sum_{m \sim \tilde{p}_T} Z_m \cos(2\theta m). \quad (\text{F.1})$$

We term this variant algorithm the Gaussian Maximum Magnitude Amplitude Estimation (GMMAE). From Fig. 9, we see that the algorithm only operates when the circuit is sufficiently deep, with low-depth circuits having a significantly higher error rate compared to GLSAE. In addition to the indiscernibility of the two Gaussian peaks, as with GLSAE, the magnitude function here has no guarantees that the function would be maximized at  $\theta = \lambda$ , whereas GLSAE has this guarantee from the nature of least square estimators. This results in a merging of the aforementioned Gaussian peaks and offsets the actual original peaks, distorting the maximum found from its original position and inducing greater errors in a wider range. Hence, the magnitude function is only used for GDMAE, where there is only one Gaussian peak.

## 2. Low-depth amplitude estimation

In Fig. 10, we show that our algorithms perform better compared to Power law AE [12] and exhibit the depth–query tradeoff when compared to Heisenberg-limited amplitude estimation. We quickly note that we do not implement the QoPrime AE algorithm due to the complexity of the post-processing algorithm, as well as due to prior numerical results that indicate an inferiority to Power law AE in practice [12, 62]. We also omit here the low-depth approaches from Rall and Fuller [8] and Vu *et al.* [13], whose algorithms require a non-Chebyshev polynomial transformation for the purposes of obtaining unbiased estimates, and which would require additional quantum resources (additional phase gates and an additional control qubit) for the implementation of QSP that would be difficult to quantify when compared to the other Grover-

type algorithms implemented in this paper.

Given that we select  $M, N \in \mathcal{O}(\epsilon^{-2/3})$ , the complexity matches that of obtaining the evolution times from a uniform grid. Under this setting, we can apply direction of arrival algorithms from classical signal processing directly, and hence we apply the ESPRIT algorithm as a benchmark, which we detail as follows:

***Off-the-shelf ESPRIT.***— As our signals are a single cosine, we can adapt Derevianko *et al.* [98]’s modified ESPRIT algorithm tailored to cosine signal extraction. Compared to Labib *et al.* [10]’s ESPRIT algorithm for amplitude estimation, standard ESPRIT does not construct virtual arrays nor does it require log-likelihood minimization for sign finding, but does require a uniform sample of the signal array. Our results in Fig. 11 show that our algorithm has comparable results to ESPRIT, which is known to be an efficient classical signal processing algorithm even in a high noise regime [81].